Available online at www.sciencedirect.com
ScienceDirect
Journal of Computational Physics 221 (2007) 349–369
JOURNAL OF COMPUTATIONAL PHYSICS
www.elsevier.com/locate/jcp

An interior penalty Galerkin method for the MHD equations in heterogeneous domains

J.-L. Guermond [a,*,1], R. Laguerre [a,b], J. Léorat [c], C. Nore [b,d]

[a] Department of Mathematics, Texas A&M University, 3368 TAMU, College Station, TX 77843-3368, USA
[b] Laboratoire d'Informatique pour la Mécanique et les Sciences de l' Ingénieur , CNRS, BP 133, 91403 Orsay Cedex, France
[c] Luth, Observatoire de Paris-Meudon, place Janssen, 92195-Meudon, France
[d] Université Paris XI, Département de Physique, 91405 Orsay Cedex, France

Received 20 February 2006; received in revised form 10 June 2006; accepted 12 June 2006
Available online 23 August 2006

Abstract

The Maxwell equations in the magnetohydrodynamic (MHD) limit in heterogeneous domains composed of conducting and non-conducting regions are solved by using Lagrange finite elements and by enforcing continuities across interfaces using an Interior Penalty technique à la Baker [Finite element methods for elliptic equations using non-conforming elements, Math. Comp. 31 (137) (1977) 45–59]. The method is shown to be stable and convergent and is validated by convergence tests. It is used to compute Ohmic decay in various compact conducting domains and to simulate the kinematic dynamo action in two different geometries.
Published by Elsevier Inc.

MSC: 76M05

Keywords: Finite elements; Discontinuous Galerkin; Magnetohydrodynamics; Dynamo action

1. Introduction

1.1. Introduction

The goal of the present paper is to introduce a finite element technique for solving the Maxwell equations in the MHD limit in heterogeneous domains. Denoting by L and T the characteristic length and time scales of interest, the MHD limit we refer to corresponds to $L/T \ll \mathfrak{c}$, where $\mathfrak{c}$ is the speed of light. In this context, the displacement currents are neglected and the electromagnetic waves are filtered out. We particularly focus our attention on domains that can be decomposed into regions with non-zero conductivity and regions with zero conductivity. We refer to [1,6] for the asymptotic analysis of this problem.

* Corresponding author.
E-mail addresses: laguerre@limsi.fr (R. Laguerre), Jacques.Leorat@obspm.fr (J. Léorat), nore@limsi.fr (C. Nore).
[1] On long leave from LIMSI (CNRS-UPR 3251), BP 133, 91403 Orsay, France.

0021-9991/$ - see front matter. Published by Elsevier Inc.
doi:10.1016/j.jcp.2006.06.045

The main mathematical difficulty arising from this situation is that the magnetic field, $\mathbf{H}$, in the non-conducting region is curl free and the electric field, $\mathbf{E}$, cannot be eliminated by using the Ohm law in this region. Many methods have been proposed to solve this problem. One technique consists of modeling the insulating region as weakly conducting and eliminating $\mathbf{E}$ using the small artificial conductivity thereof, see e.g. [18]. This is a penalty method which is known to be ill-conditioned and to be unable to account for induced charge problems as occurring in the so-called Faraday disk. Alternative algorithms involving vector potentials for the magnetic field or for the electric current have also been proposed (see for example [4,12]). Another approach consists of realizing that $\mathbf{E}$ in the non-conducting region is the Lagrange multiplier associated with the constraint $\nabla \times \mathbf{H} = 0$, as emphasized in [15,16]. It then becomes clear that if both $\mathbf{E}$ and $\mathbf{H}$ are retained as dependent variables, the problem has a saddle point structure. If finite elements are used, this implies that either mixed pairs of finite elements (see e.g. [14–16]) or a stabilization method (e.g. Galerkin/least-squares, sub-grid viscosity, discontinuous Galerkin, etc.) must be employed. The former method has been shown to be efficient in two space dimensions in [14], but it turns out that retaining both $\mathbf{H}$ and $\mathbf{E}$ in the non-conducting region is somewhat computationally expensive in three space dimensions.

The above reasons have led us to shift our focus on methods that are based on $\mathbf{H}$ in the conducting region and on a magnetic scalar potential in vacuum. In fact, if the external insulating domain is simply connected, the magnetic field thereof can be expressed in terms of a harmonic scalar potential ϕ. It is then possible to reduce the dynamical variables to $\mathbf{H}$ in the conducting region and to ϕ in the insulating exterior. A further reduction is possible in principle by using boundary elements to solve the external harmonic problem. This method has been introduced in [5] and shown in [17] to work well for solving the ohmic diffusion equation. However, it remains to be validated with the kinematic dynamo and the full nonlinear MHD equations, which is the focus of our group. If the boundary elements reduction alluded to above is not done, a serious question concerning the coupling of the two representations of the magnetic field arises. The tangential component of $\mathbf{H}$ must match the tangential component of $\nabla\phi$ across the interface between the conducting and non-conducting regions. Likewise, the normal component of $\mu^c\mathbf{H}$ must also match the normal component of $\mu^v\nabla\phi$ across this interface, where μ^c, μ^v are the magnetic permeabilities in the conducting and non-conducting regions, respectively. As shown by Bossavit [6], it turns out that when using Nédélec finite elements (also called edge elements) the above coupling is natural. However, if Lagrange elements are used, this coupling becomes a serious mathematical headache. The first mathematical difficulty is that when strongly enforcing tangential boundary conditions on Lagrange elements, it may happen that a singular component of the solution is not computed if the interface is not smooth (see Costabel's lemma [10]).[2] Another issue is that exact coupling may sometimes be impossible when using polynomials to approximate $\mathbf{H}$ and ϕ. These reasons and the fact that we nevertheless insist on working with Lagrange elements have lead us to consider an Interior Penalty technique [3] to weakly enforce the coupling across the interface.

The method under consideration in the present paper consists of working with the pair $\mathbf{H}$–ϕ. We use Lagrange elements of degree $k \geqslant 1$ to approximate $\mathbf{H}$ in the conducting region, and we use Lagrange elements of degree $k+1 \geqslant 2$ to approximate ϕ in the non-conducting region. The tangential component of the magnetic field is weakly enforced to be continuous across the interface by a consistent Interior Penalty method. The normal component of the magnetic induction is naturally (i.e., not particularly taken care of) enforced to be continuous across the interface by the weak formulation. The method is shown to be stable and convergent and is validated on three-dimensional benchmark problems.

The paper is organized as follows. We introduce the setting and a weak formulation of the problem under consideration in Section 2. The Interior Penalty Galerkin approximation technique that we propose to solve the problem together with its stability and error analysis is presented in Section 3. Technical details and convergence tests confirming our a priori error analysis are reported in Section 4. In Section 5, we demonstrate the capability of the method by studying ohmic diffusion in different geometries and two examples of kinematic dynamo action. Concluding remarks are reported in Section 6.

[2] $\mathbf{H}^1(\Omega) \cap \mathbf{H}_{0,\mathrm{curl}}(\Omega)$ is a genuine closed subspace of $\mathbf{H}_{0,\mathrm{curl}}(\Omega) \cap \mathbf{H}_{\mathrm{div}}(\Omega)$ if Ω is a non-convex polyhedron.

2. The continuous problem

2.1. The setting

Let us consider the MHD limit of the Maxwell equations in an open, connected, domain $\Omega \subset \mathbb{R}^3$:

$$\begin{cases} \mu \partial_t \mathbf{H} = -\nabla \times \mathbf{E} & \text{in } \Omega, \\ \nabla \times \mathbf{H} = \sigma(\mathbf{E} + \mathbf{u} \times \mu \mathbf{H}) + \mathbf{j}^s & \text{in } \Omega, \\ \mathbf{E} \times \mathbf{n}|_\Gamma = \mathbf{a}, \quad \mathbf{H}|_{t=0} = \mathbf{H}_0, \end{cases} \tag{2.1}$$

where $\mathbf{j}^s$ is an externally imposed distribution of current, $\mathbf{u}$ an imposed velocity field, $\mathbf{a}$ a given boundary data, $\mathbf{H}_0$ an initial magnetic field, μ the permeability field, and σ the conductivity field. In the above formulation the displacement currents represented by the term $\epsilon \partial_t \mathbf{E}$ in the Ampère–Maxwell equation has been neglected due to the fact that $\mathbf{u}$ scales like L/T and the scales of interest L and T are such that $L/(cT)$ is extremely small. Note also that this formulation is valid only if σ is uniformly positive over Ω and in this case an evolution equation for $\mathbf{H}$ can be obtained after eliminating the electric field.

Additional terms must be accounted for in (2.1) when σ is not uniformly positive, as we now explain, To be more specific, the domain is henceforth assumed to be bounded and its boundary Γ to be at least Lipschitz continuous. Ω is assumed to be partitioned into a conducting region (subscript c) and an insulating region (subscript v) as follows:

$$\bar{\Omega} = \bar{\Omega}_c \cup \bar{\Omega}_v, \quad \Omega_c \cap \Omega_v = \emptyset, \tag{2.2}$$

where the overbar $\overline{(\cdot)}$ denotes the closure. We henceforth assume that the conductivity $\sigma(x)$ is zero in Ω_v and is bounded from below and from above in Ω_c by positive constants, say σ_0 and σ_1, respectively. For instance the conducting medium occupying Ω_c could be the Earth core, the solar plasma, molten metals (gallium, sodium), or any other conducting material. The insulating region, Ω_v, could be for instance vacuum, the Earth mantle, or air. To refer to boundary conditions easily, we introduce

$$\Gamma_c = \partial\Omega \cap \partial\Omega_c, \quad \Gamma_v = \partial\Omega \cap \partial\Omega_v, \quad \Gamma = \partial\Omega = \Gamma_v \cup \Gamma_c.$$

Moreover, we denote by Γ_v^0 the connected component of $\partial\Omega_v$ that contains Γ_v. We assume that $\partial\Omega_v$ has $J+1$ connected components, say

$$\Gamma_v^0, \Gamma_v^1, \ldots, \Gamma_v^J.$$

Fig. 1 presents a particular setting with $J = 2$.

The interface between the conducting region and the non-conducting region is denoted by

$$\Sigma = \partial\Omega_c \cap \partial\Omega_v.$$

When σ and $\mathbf{j}^s$ are simultaneously zero somewhere in the domain, say in Ω_v, the problem (2.1) must be replaced by:

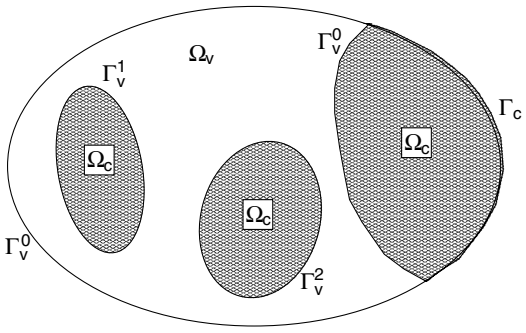

Fig. 1. Computational domain Ω with its different boundaries: the shaded regions constitute the conducting domain Ω_c, the non-shaded domain is the vacuum Ω_v.

$$\begin{cases} \mu\partial_t \mathbf{H} = -\nabla\times\mathbf{E} & \text{in } \Omega, \\ \nabla\times\mathbf{H} = \begin{cases} \sigma(\mathbf{E}+\mathbf{u}\times\mu\mathbf{H})+\mathbf{j}^s & \text{in } \Omega_c, \\ 0 & \text{in } \Omega_v, \end{cases} & \\ \nabla\cdot\mathbf{E} = 0 & \text{in } \Omega_v, \\ \mathbf{E}\times\mathbf{n}|_\Gamma = \mathbf{a}, \quad \mathbf{H}|_{t=0} = \mathbf{H}_0, & \\ \int_{\Gamma_v^i} \mathbf{E}\cdot\mathbf{n} = 0, \quad 1\leqslant i\leqslant J & \end{cases} \tag{2.3}$$

where $\Gamma_v^0, \Gamma_v^1, \ldots, \Gamma_v^J$ are the $J+1$ connected components of $\partial\Omega_v$ as defined above. We refer to [1,6] for more details on the asymptotic analysis leading to this model. Note that the condition $\int_{\Gamma_v^0}\mathbf{E}\cdot\mathbf{n}=0$ needs not be enforced since it is a consequence of the J other conditions together with $\mathbf{E}$ being solenoidal. Observe that the two extra conditions $\nabla\cdot\mathbf{E}|_{\Omega_v}=0$ and $\int_{\Gamma_v^i}\mathbf{E}\cdot\mathbf{n}=0,\ 1\leqslant i\leqslant J$ are what is left from the Ampère–Maxwell equation when passing to the limit to zero on the ratio $L/(cT)$ assuming that there is no electrostatic charge distributed in the domain. These extra conditions ensure that $\mathbf{E}$ is uniquely defined, i.e., they have no effect on $\mathbf{H}$.

2.2. Introduction of ϕ and elimination of E

If in addition to the above hypotheses on Ω, we assume that Ω_v is simply connected, the condition $\nabla\times\mathbf{H}|_{\Omega_v}=0$ implies there is a scalar potential ϕ, defined up to an arbitrary constant, such that $\mathbf{H}|_{\Omega_v}=\nabla\phi$. Moreover, if the initial data $\mathbf{H}_0$ are such that $\nabla\times\mathbf{H}_0|_{\Omega_v}=0$, we can also define ϕ_0 such that $\mathbf{H}_0|_{\Omega_v}=\nabla\phi_0$. By inserting the above definitions into (2.3) and by setting $\mathbf{E}^c=\mathbf{E}|_{\Omega_c}$, $\mathbf{E}^v=\mathbf{E}|_{\Omega_c}$, $\mathbf{H}^c=\mathbf{H}|_{\Omega_c}$, $\mu^c=\mu|_{\Omega_c}$, $\mu^v=\mu|_{\Omega_v}$, we infer that $\mathbf{H}^c$, $\mathbf{E}^c$, $\mathbf{E}^v$, ϕ solve

$$\begin{cases} \mu^c\partial_t\mathbf{H}^c = -\nabla\times\mathbf{E}^c, & \nabla\times\mathbf{H}^c = \sigma(\mathbf{E}^c+\mathbf{u}\times\mu^c\mathbf{H}^c)+\mathbf{j}^s & \text{in } \Omega_c, \\ \mu^v\partial_t\nabla\phi = -\nabla\times\mathbf{E}^v, & \nabla\cdot\mathbf{E}^v = 0 & \text{in } \Omega_v, \\ \mathbf{H}^c\times\mathbf{n}^c + \nabla\phi\times\mathbf{n}^v = 0, & \mathbf{E}^c\times\mathbf{n}^c + \mathbf{E}^v\times\mathbf{n}^v = 0 & \text{on } \Sigma, \\ \mathbf{E}^c\times\mathbf{n}^c|_{\Gamma_c} = \mathbf{a}|_{\Gamma_c}, & \mathbf{E}^v\times\mathbf{n}^v|_{\Gamma_v} = \mathbf{a}|_{\Gamma_v}, & \\ \int_{\Gamma_v^i}\mathbf{E}\cdot\mathbf{n}=0, & 1\leqslant i\leqslant J, & \\ \mathbf{H}^c|_{t=0} = \mathbf{H}_0^c, & \phi|_{t=0}=\phi_0. & \end{cases} \tag{2.4}$$

Note that the condition $(\mathbf{H}^c\times\mathbf{n}^c+\nabla\phi\times\mathbf{n}^v)|_\Sigma=0$ is meant to ensure that the curl of the field

$$\mathbf{H} = \begin{cases} \mathbf{H}^c & \text{in } \Omega_c, \\ \nabla\phi & \text{in } \Omega_v \end{cases}$$

has no singular measure concentrated on Σ. The analogous condition $(\mathbf{E}^c\times\mathbf{n}^c+\mathbf{E}^v\times\mathbf{n}^v)|_\Sigma=0$ ensures the same property for the curl of $\mathbf{E}$.

The arbitrariness of ϕ up to a constant can be removed by enforcing ϕ to be of zero mean, say $\int_{\Omega_v}\phi=0$.

Assuming enough regularity is at hand, we now formally eliminate $\mathbf{E}$ by proceeding as follows: we use Ohm's law to eliminate $\mathbf{E}^c$ from Faraday's equation in the conducting region. We take the divergence of Faraday's equation in the non-conducting medium to get rid of $\nabla\times\mathbf{E}^v$. We eliminate the tangential component of $\mathbf{E}$ on Γ_v by using the following representation $\mathbf{E}^v|_{\Gamma_v}=(\mathbf{E}^v\cdot\mathbf{n}^v)\mathbf{n}^v+\mathbf{n}^v\times\mathbf{a}$. Finally, we obtain:

$$\begin{cases} \mu^c\partial_t\mathbf{H}^c = -\nabla\times\left(\frac{1}{\sigma}(\nabla\times\mathbf{H}^c-\mathbf{j}^s)-\mathbf{u}\times\mu^c\mathbf{H}^c\right) & \text{in } \Omega_c, \\ \mu^v\partial_t\Delta\phi = 0 & \text{in } \Omega_v, \\ (\nabla\times\mathbf{H}^c-\sigma\mathbf{u}\times\mu\mathbf{H}^c)\times\mathbf{n}^c = \sigma\mathbf{a}+\mathbf{j}^s\times\mathbf{n}^c & \text{on } \Gamma_c, \\ \mu^v\partial_{\mathbf{n}^v}(\partial_t\phi) = -\mathbf{n}^v\cdot\nabla\times(\mathbf{n}^v\times\mathbf{a}) & \text{on } \Gamma_v, \\ \mathbf{H}^c\times\mathbf{n}^c+\nabla\phi\times\mathbf{n}^v=0 & \text{on } \Sigma, \\ \mu^c\mathbf{H}^c\cdot\mathbf{n}^c+\mu^v\nabla\phi\cdot\mathbf{n}^v=0 & \text{on } \Sigma, \\ \mathbf{H}^c|_{t=0}=\mathbf{H}_0^c, \quad \phi|_{t=0}=\phi_0. & \end{cases} \tag{2.5}$$

Observe that the operator $\mathbf{n}^v \cdot \nabla \times (\cdot)$ involves only tangential derivatives; hence, it is meaningful to have it acting on the field $\mathbf{n}^v \times \mathbf{a}$ which is only defined on Γ. Note also that $(\mu^c \mathbf{H}^c \cdot \mathbf{n}^c + \mu^v \nabla\phi \cdot \mathbf{n}^v)|_\Sigma = 0$ express the continuity of the normal component of the magnetic induction across Σ. This equation is a consequence of the continuity of the tangential component of the electric field. If the electric field is needed, it is computed in the conducting domain by using Ohm's law, and it is determined in the non-conducting medium by solving the Cauchy–Riemann problem: $\nabla \times \mathbf{E}^v = -\mu^v \partial_t \nabla\phi$, $\nabla \cdot \mathbf{E}^v = 0$, $\mathbf{E}^v \times \mathbf{n}^v|_\Sigma = -\mathbf{E}^c \times \mathbf{n}^c|_\Sigma$, $\mathbf{E}^v \times \mathbf{n}|_\Gamma = \mathbf{a}$, and $\int_{\Gamma_v^i} \mathbf{E}^v \cdot \mathbf{n} = 0$, $1 \leqslant i \leqslant J$.

2.3. Weak formulation

Let us now construct a weak formulation for problem (2.5). We henceforth assume that $\mathbf{u} \in L^\infty(0,+\infty; \mathbf{L}^2(\Omega_c))$ and $\mathbf{j}^s \in L^\infty(0,+\infty;\mathbf{L}^2(\Omega_c))$. Likewise we assume that σ and μ^c are both in $L^\infty(0,+\infty;L^\infty(\Omega_c))$ and μ^v is in $L^\infty(0,+\infty;L^\infty(\Omega_v))$. Being given a normed space $E, L^p(0,+\infty;E)$ is the set of the functions that map the time interval $(0,+\infty)$ to E and whose norm in E is L^p integrable, $1 \leqslant p \leqslant +\infty$. More generally, we denote by $W^{s,p}(0,+\infty;E)$ the subspace of $L^p(0,+\infty;E)$ whose members are differentiable with respect to time up to the order s, and the time derivatives in question have norms in E that are L^p integrable. To alleviate notation, we use the notation $(\mathbf{f},\mathbf{g})_E$ to denote the integral $\int_E \mathbf{f} \cdot \mathbf{g}$, where E is any measurable subset of Ω or $\Gamma_v \cup \Gamma_c$.

Instead of working directly with (2.5) it turns out that it is more straightforward to construct the weak formulation starting from (2.4) and eliminating $\mathbf{E}$ on the fly. Let $\mathbf{b} \in \mathbf{H}_{\mathrm{curl}}(\Omega_c)$ be a test function. After multiplying the Faraday equation by $\mathbf{b}$ in Ω_c in (2.4), integrating over Ω_c, and integrating by parts, we obtain

$$(\mu^c \partial_t \mathbf{H}^c, \mathbf{b})_{\Omega_c} + (\mathbf{E}^c, \nabla \times \mathbf{b})_{\Omega_c} + (\mathbf{E}^c, \mathbf{b} \times \mathbf{n}^c)_\Sigma = (\mathbf{E}^c \times \mathbf{n}^c, \mathbf{b})_{\Gamma_c}.$$

Then using Ohm's law in Ω_c and using the boundary conditions on $\mathbf{E}^c$ yields

$$\begin{aligned}(\mu^c \partial_t \mathbf{H}^c, \mathbf{b})_{\Omega_c} + \left(\frac{1}{\sigma}\nabla \times \mathbf{H}^c, \nabla \times \mathbf{b}\right)_{\Omega_c} + \left(\frac{1}{\sigma}\nabla \times \mathbf{H}^c, \mathbf{b} \times \mathbf{n}^c\right)_\Sigma \\ = \left(\frac{1}{\sigma}\mathbf{j}^s + \mathbf{u} \times \mu^c \mathbf{H}^c, \nabla \times \mathbf{b}\right)_{\Omega_c} + \left(\frac{1}{\sigma}\mathbf{j}^s + \mathbf{u} \times \mu^c \mathbf{H}^c, \mathbf{b} \times \mathbf{n}^c\right)_\Sigma + (\mathbf{a}, \mathbf{b}).\end{aligned} \tag{2.6}$$

Likewise by using $\nabla\psi$, $\psi \in H^1(\Omega_v)$, to test the Faraday equation in Ω_v in (2.4), we obtain

$$(\mu^v \partial_t \nabla\phi, \nabla\psi)_{\Omega_v} - (\mathbf{E}^v \times \mathbf{n}^v, \nabla\psi)_\Sigma = (\mathbf{E}^c \times \mathbf{n}^c, \nabla\psi)_{\Gamma_v}.$$

By using again the boundary condition together with the fact that

$$\mathbf{E}^v \times \mathbf{n}^v|_\Sigma = -\mathbf{E}^c \times \mathbf{n}^c|_\Sigma = -\left(\frac{1}{\sigma}(\nabla \times \mathbf{H}^c - \mathbf{j}^s) - \mathbf{u} \times \mu^c \mathbf{H}^c\right) \times \mathbf{n}^c|_\Sigma,$$

we infer

$$(\mu^v \partial_t \nabla\phi, \nabla\psi)_{\Omega_v} + \left(\frac{1}{\sigma}(\nabla \times \mathbf{H}^c - \mathbf{j}^s) - \mathbf{u} \times \mu^c \mathbf{H}^c, \nabla\psi \times \mathbf{n}^v\right)_\Sigma = (\mathbf{a}, \nabla\psi)_{\Gamma_v}. \tag{2.7}$$

For the above developments to make sense we now specify the regularity we expect to hold on $\mathbf{H}^c$ and ϕ by introducing

$$\mathbf{L} = \left\{(\mathbf{b},\psi) \in \mathbf{L}^2(\Omega_c) \times H^1_{\int=0}(\Omega_v)\right\}, \tag{2.8}$$

$$\mathbf{X} = \left\{(\mathbf{b},\psi) \in \mathbf{H}_{\mathrm{curl}}(\Omega_c) \times H^1_{\int=0}(\Omega_v); (\mathbf{b} \times \mathbf{n}^c + \nabla\psi \times \mathbf{n}^v)|_\Sigma = 0\right\}, \tag{2.9}$$

and we equip $\mathbf{L}$ and $\mathbf{X}$ with the norm of $\mathbf{L}^2(\Omega_c) \times H^1(\Omega_v)$ and $\mathbf{H}_{\mathrm{curl}}(\Omega_c) \times H^1(\Omega_v)$, respectively. Here, $H^1(\Omega_v)$ is the space of the scalar-valued functions on Ω_v that are L^2-integrable and whose partial derivatives are also L^2-integrable. $H^1_{\int=0}(\Omega_v)$ is the subspace of $H^1(\Omega_v)$ composed of the functions of zero mean value. Recall that owing to the Poincaré–Friedrichs inequality $\|\nabla\phi\|_{L^2(\Omega_v)}$ is a norm equivalent to that of $H^1(\Omega_v)$. The space $\mathbf{H}_{\mathrm{curl}}(\Omega_c)$ is composed of the vector-valued functions on Ω_c that are componentwise L^2-integrable and whose

curl is also componentwise L^2-integrable. The space $\mathbf{H}_{\mathrm{div}}(\Omega)$ is composed of the vector-valued functions on Ω that are componentwise L^2-integrable and whose divergence is L^2-integrable.

By adding (2.6) and (2.7) we obtain that the pair $(\mathbf{H}^c,\phi)$ solves

$$\begin{aligned}&(\mu^c\partial_t\mathbf{H}^c,\mathbf{b})_{\Omega_c}+(\mu^v\partial_t\nabla\phi,\nabla\psi)_{\Omega_v}+\left(\frac{1}{\sigma}(\nabla\times\mathbf{H}^c-\mathbf{j}^s)-\mathbf{u}\times\mu^c\mathbf{H}^c,\nabla\times\mathbf{b}\right)_{\Omega_c}\\&\quad+\left(\frac{1}{\sigma}(\nabla\times\mathbf{H}^c-\mathbf{j}^s)-\mathbf{u}\times\mu^c\mathbf{H}^c,\mathbf{b}\times\mathbf{n}^c+\nabla\psi\times\mathbf{n}^v\right)_{\Sigma}\\&=(\mathbf{a},\mathbf{b})_{\Gamma_c}+(\mathbf{a},\nabla\psi)_{\Gamma_v}.\end{aligned}\tag{2.10}$$

Observe that the term $(\frac{1}{\sigma}(\mathbf{H}^c-\mathbf{j}^s)-\mathbf{u}\times\mu^c\mathbf{H}^c,\mathbf{b}\times\mathbf{n}^c+\nabla\psi\times\mathbf{n}^v)_{\Sigma}$ is zero whenever the pair of test functions $(\mathbf{b},\psi)$ is a member of $\mathbf{X}$. This term will play a major role when it comes to constructing a non-conforming approximation to the problem, see Section 3.1.

Let us denote by X' the dual of the Hilbert space $\mathbf{X}$. We are now in measure to formulate the problem as follows: Seek the pair $(\mathbf{H}^c,\phi)\in L^2(0,+\infty;\mathbf{X})\cap L^\infty(0,+\infty,\mathbf{L})$ with $(\partial_t\mathbf{H}^c,\partial_t\phi)\in L^2(0,+\infty;\mathbf{X}')$ such that for all $(\mathbf{b},\psi)\in X$ and a.e. $t\in(0,+\infty)$,

$$\begin{aligned}&\mathbf{H}^c|_{t=0}=\mathbf{H}_0^c,\quad \nabla\phi|_{t=0}=\nabla\phi_0,\\&(\mu^v\partial_t\mathbf{H}^c,b)_{\Omega_c}+(\mu^v\partial_t\nabla\phi,\nabla\psi)_{\Omega_v}+\left(\frac{1}{\sigma}\nabla\times\mathbf{H}^c-\mathbf{u}\times\mu^c\mathbf{H}^c,\nabla\times\mathbf{b}\right)_{\Omega_c}\\&\quad=\left(\frac{1}{\sigma}\mathbf{j}^s,\nabla\times\mathbf{b}\right)_{\Omega_c}+(\mathbf{a},\mathbf{b})_{\Gamma_c}+(\mathbf{a},\nabla\psi)_{\Gamma_v}.\end{aligned}\tag{2.11}$$

To alleviate notation, let us define the following bilinear form

$$a((\mathbf{b},\psi),(\mathbf{h},\varphi))=\left(\frac{1}{\sigma}\nabla\times\mathbf{b}-\mathbf{u}\times\mu^c\mathbf{b},\nabla\times\mathbf{h}\right)_{\Omega_c},\quad(\mathbf{b},\psi),(\mathbf{h},\varphi)\in X.\tag{2.12}$$

Lemma 2.1. *Under the assumptions above on σ and μ^c, there are $\gamma\geqslant 0$ and $c>0$ s.t.*

$$\forall(\mathbf{b},\psi)\in\mathbf{X},\quad a((\mathbf{b},\psi),(\mathbf{b},\psi))+\gamma(\|\mathbf{b}\|^2_{\mathbf{L}^2(\Omega_c)}+\|\nabla\psi\|^2_{\mathbf{L}^2(\Omega_v)})\geqslant c\|(\mathbf{b},\psi)\|^2_{\mathbf{X}}.$$

Proof. Let us set $c(\mathbf{u},\mu)=\|\mathbf{u}\|_{L^\infty(\Omega_c)}\|\mu^c\|_{L^\infty(\Omega_c)}$ and $\gamma=c(\mathbf{u},\mu)^2\sigma_1$. Then for all $(\mathbf{b},\psi)\in\mathbf{X}$, the following holds:

$$\begin{aligned}a((\mathbf{b},\psi),(\mathbf{b},\psi))&\geqslant\frac{1}{\sigma^1}\|\nabla\times\mathbf{H}\|^2_{\mathbf{L}^2(\Omega_c)}-c(\mathbf{u},\mu)\|\mathbf{H}\|_{\mathbf{L}^2(\Omega_c)}\|\nabla\times\mathbf{H}\|_{\mathbf{L}^2(\Omega_c)}\\&\geqslant\frac{1}{2\sigma_1}\|\nabla\times\mathbf{H}\|^2_{\mathbf{L}^2(\Omega_c)}-c(\mathbf{u},\mu)^2\frac{\sigma_1}{2}\|\mathbf{H}\|^2_{\mathbf{L}^2(\Omega_c)}.\end{aligned}$$

Clearly,

$$a((\mathbf{b},\psi),(\mathbf{b},\psi))+\gamma\|(\mathbf{b},\psi)\|^2_{\mathbf{L}}\geqslant\min\left(\frac{1}{2\sigma_1},c(\mathbf{u},\mu)^2\frac{\sigma_1}{2}\right)\|(\mathbf{b},\psi)\|^2_{\mathbf{X}}.\qquad\square$$

Note that in the real nonlinear MHD situation, $\mathbf{u}$ solves the Navier–Stokes equations, and the magnetic energy produced by the velocity-induced currents exactly balances the kinetic energy produced by the Lorentz force in the momentum equation (i.e., $-((\nabla\times\mathbf{H}^c)\times\mu^c\mathbf{H}^c,\mathbf{u})_{\Omega_c}$). In other words, the bothering term (i.e., $-(\mathbf{u}\times\mu^c\mathbf{H}^c,\nabla\times\mathbf{H}^c)_{\Omega_c}$) in the above lemma is exactly compensated by $-((\nabla\times\mathbf{H}^c)\times\mu^c\mathbf{H}^c,\mathbf{u})_{\Omega_c}$ which is obtained by testing the momentum equation with $\mathbf{u}$.

Theorem 2.1. *The problem (2.11) is wellposed.*

Proof. Owing to the coercivity property stated in Lemma 2.1, Lions' theorem (see e.g. [8, p. 218; 21, pp. 253–258]) ensures that problem (2.11) has a unique solution. $\square$

2.4. Stabilized weak formulation

It is clear from (2.4) that if $\mathbf{H}_0^c$ is solenoidal, $\mathbf{H}^c$ stays solenoidal for all times. Note, however, that $\nabla\cdot\mathbf{H}^c=0$ is not part of the system defining the magnetic field but is merely a consequence of Faraday's equation. Nevertheless, provided $\nabla\cdot\mathbf{H}_0^c=0$, it is quite common to transform $\nabla\cdot\mathbf{H}^c=0$ into a constraint by replacing Faraday's equation in Ω_c in (2.4) by

$$\mu^c\partial_t\mathbf{H}^c=-\nabla\times\mathbf{E}^c+\mu^c\nabla(\alpha\nabla\cdot\mu^c\mathbf{H}^c), \tag{2.13}$$

$$\nabla\cdot(\mu^c\mathbf{H}^c)|_{\Gamma_c}=0, \tag{2.14}$$

where $\alpha=\alpha(x)$ is a user-defined scalar-valued function (a constant may do the job), which must be positive, uniformly bounded from above, uniformly bounded away from zero from below, and should be chosen so that the magnitude of the two terms in the right-hand side are balanced. Henceforth we assume $\alpha(x)\geqslant\alpha_0>$ for all $x\in\Omega_c$. Consequently, without any additional difficulty, we shall henceforth consider a modified (i.e., stabilized) version of the problem (2.11) by replacing the bilinear form a by the following one:

$$\tilde{a}((\mathbf{b},\psi),(\mathbf{h},\varphi))=a((\mathbf{b},\varphi),(\mathbf{h},\varphi))+(\alpha\nabla\cdot\mu^c\mathbf{b},\nabla\cdot\mu^c\mathbf{h})_{\Omega_c}. \tag{2.15}$$

3. Finite element approximation

We now approximate the problem (2.11) by using finite elements. The key feature of the method that we propose is that the continuity of the tangential component of the magnetic field across Σ is enforced weakly by using an interior penalty technique. This technique is the work horse of discontinuous Galerkin approximation methods for elliptic and parabolic equations [2,3].

3.1. The interior penalty Galerkin approximation

Let $\{\mathscr{T}_h^c\}_{h>0}$ and $\{\mathscr{T}_h^v\}_{h>0}$ be regular families of non-overlapping meshes for Ω_c and Ω_v, respectively. For the sake of simplicity we assume that the meshes are composed of simplices and the interface between the two non-overlapping meshes $\mathscr{T}_h^c$ and $\mathscr{T}_h^v$ is Σ. Let k and k' be two positive integers. The approximation space for the magnetic field and the scalar potential is denoted by $\mathbf{X}_h=\mathbf{X}_h^{\mathbf{H}}\times X_h^{\phi}$ and defined as follows:

$$\mathbf{X}_h=\{(\mathbf{b},\psi)\in\mathscr{C}^0(\overline{\Omega_c})\times\mathscr{C}^0(\overline{\Omega_v});\mathbf{b}|_K\in\mathbb{P}_k,\forall K\in\mathscr{T}_h^c;\psi|_K\in\mathbb{P}_{k'},\forall K\in\mathscr{T}_h^v\}, \tag{3.1}$$

where $\mathbb{P}_{k'}$ denotes the vector space of the scalar-valued polynomials of total degree at most k', and $\mathbb{P}_k$ denotes the vector space of the vector-valued polynomials of total degree at most k. We shall also use the space $\mathbf{X}_{(h)}=[\mathbf{H}^1(\Omega_c)\times H^2(\Omega_v)]+\mathbf{X}_h$, where $H^2(\Omega_v)$ is the space of the scalar-valued functions on Ω_v that are in $H^1(\Omega_v)$ and whose second-order partial derivatives are square integrable. Observe that for any given pair $(\mathbf{b},\psi)$ in $\mathbf{X}_h$ we do not enforce the tangent component of $\mathbf{b}$ to match that of the gradient of ψ across Σ. Actually, enforcing such a match would be impossible in most practical situations unless $\mathbf{X}_h$ is composed of the so-called edge elements or Nédélec elements. Since we do not want to use edge elements, the matching in question will be enforced weakly as explained below.

Since the solution to (2.11) also satisfies (2.10) where the test functions $\mathbf{b}$ and ψ may be discontinuous, we define the following bilinear form on $\mathbf{X}_{(h)}\times\mathbf{X}_h$:

$$\begin{aligned}a_h((\mathbf{h},\varphi),(\mathbf{b},\psi))=\tilde{a}((\mathbf{h},\varphi),(\mathbf{b},\psi))&+\left(\frac{1}{\sigma}\nabla\times\mathbf{h}-\mathbf{u}\times\mu\mathbf{h},(\mathbf{b}\times\mathbf{n}^c+\nabla\psi\times\mathbf{n}^v)\right)_{\Sigma}\\&+\beta\left(\frac{1}{h}(\mathbf{h}\times\mathbf{n}^c+\nabla\varphi\times\mathbf{n}^v),(\mathbf{b}\times\mathbf{n}^c+\nabla\psi\times\mathbf{n}^v)\right)_{\Sigma}.\end{aligned} \tag{3.2}$$

The parameter $\beta>0$ is a tunable constant and h denotes the typical mesh size. The second term in the right-hand side of (3.2) is the consistency term already present in (2.10). As already mentioned earlier, this term vanishes whenever $\mathbf{b}\times\mathbf{n}^c+\nabla\psi\times\mathbf{n}^v$ is zero on Σ. The last term is a penalty term. It is meant to constrain the jump of the tangential component of the approximate magnetic field across Σ to be small.

Let $[0,T]$ be some given interval. Let $(\mathbf{H}_{0,h}^c, \phi_{0,h}) \in \mathbf{X}_h$ be approximations of $\mathbf{H}_0^c$ and ϕ_0, respectively. The semi-discrete problem is formulated as follows: Seek $(\mathbf{H}_h^c, \phi_h) \in \mathscr{C}^1([0,T];\mathbf{X}_h)$ such that for all $(\mathbf{b},\psi) \in \mathbf{X}_h$ and all $t \in [0,T]$,

$$\begin{aligned}(\mathbf{H}_h^c, \phi_h)|_{t=0} &= (\mathbf{H}_{0,h}^c, \phi_{0,h}), \quad (\mu^c \partial_t \mathbf{H}_h, \mathbf{b})_{\Omega_c} + (\mu^v \nabla \partial_t \phi_h, \nabla\psi)_{\Omega_v} + a_h((\mathbf{H}_h^c, \phi_h), (\mathbf{b},\psi)) \\ &= J((\mathbf{H}_h^c, \phi_h), (\mathbf{b},\psi)),\end{aligned} \tag{3.3}$$

where the source term is given by

$$J((\mathbf{H}_h^c, \phi_h), (\mathbf{b},\psi)) = \left(\frac{1}{\sigma}\mathbf{j}^s, \nabla\times\mathbf{b}\right)_{\Omega_c} + \left(\frac{1}{\sigma}\mathbf{j}^s, \mathbf{b}\times\mathbf{n}^c + \nabla\psi\times\mathbf{n}^v\right)_{\Sigma} + (\mathbf{a},\mathbf{b})_{\Gamma_c} + (\mathbf{a},\nabla\psi)_{\Gamma_v}. \tag{3.4}$$

The error analysis will show that β must be taken large enough for the method to be convergent. This feature is characteristic of Interior Penalty methods. It would have been possible to overcome this slight inconvenience by using a local discontinuous Galerkin (LDG) approach, [9,23]. We preferred not using this approach since LDG requires solving local problems.

3.2. Error analysis

We perform the error analysis of problem (3.3) in this section.

Before stating the main convergence result, we define appropriate interpolation operators. For all $\mathbf{H}^c \in \mathscr{C}^1(0,T;\mathbf{H}^1(\Omega_c))$ we define $\pi_h\mathbf{H}^c \in \mathscr{C}^1(0,T;\mathbf{X}_h^{\mathbf{H}})$ so that $\pi_h\mathbf{H}^c|_{t=0} = \mathscr{I}_h\mathbf{H}^c|_{t=0}$ where $\mathscr{I}_h$ is an interpolation operator with optimal interpolation properties (e.g. Lagrange, Clément, or Scott–Zhang interpolation operators.), and for all $\mathbf{b} \in \mathbf{X}_h^{\mathbf{H}}$ and for a.e. $t \in (0,T)$,

$$\begin{aligned}&(\mu^c \partial_t \pi_h\mathbf{H}^c, \mathbf{b})_{\Omega_c} + \left(\frac{1}{\sigma}\nabla\times\pi_h\mathbf{H}^c, \nabla\times\mathbf{b}\right)_{\Omega_c} + (\alpha\nabla\cdot(\mu^c\pi_h\mathbf{H}^c), \nabla\cdot(\mu^c\mathbf{b}))_{\Omega_c} \\ &= (\mu^c\partial_t\mathbf{H}^c, \mathbf{b})_{\Omega_c} + \left(\frac{1}{\sigma}\nabla\times\mathbf{H}^c, \nabla\times\mathbf{b}\right)_{\Omega_c} + (\alpha\nabla\cdot(\mu^c\mathbf{H}^c), \nabla\cdot(\mu^c\mathbf{b}))_{\Omega_c}.\end{aligned} \tag{3.5}$$

We henceforth assume that the following approximation result holds: There are $k_1 \geqslant k_2 > 0$ such that

$$\|\pi_h\mathbf{H}^c - \mathbf{H}^c\|_{L^\infty(0,T;\mathbf{L}^2(\Omega_c))} + \|(\pi_h\mathbf{H}^c - \mathbf{H}^c)\times\mathbf{n}^c\|_{L^2(0,T;\mathbf{L}^2(\Sigma))} \leqslant ch^{k_1}\|\mathbf{H}^c\|_{\mathbf{Ho}}, \tag{3.6}$$

$$\begin{aligned}&|\nabla\times(\pi_h\mathbf{H}^c - \mathbf{H}^c)\|_{L^2(0,T;\mathbf{L}^2(\Omega_c))} + \|\nabla\cdot(\pi_h\mathbf{H}^c - \mathbf{H}^c)\|_{L^2(0,T;\mathbf{L}^2(\Omega_c))} + \|\nabla\times(\pi_h\mathbf{H}^c - \mathbf{H}^c)\times\mathbf{n}^c\|_{L^2(0,T;\mathbf{L}^2(\Sigma))} \\ &\leqslant ch^{k_2}\|\mathbf{H}^c\|_{\mathbf{Ho}},\end{aligned} \tag{3.7}$$

where $\|\cdot\|_{\mathbf{Ho}}$ is a norm involving high-order space derivatives, for instance $\|\mathbf{H}^c\|_{\mathbf{Ho}} = \|\mathbf{H}^c\|_{L^\infty(0,T;\mathbf{W}^{k_1+1,\infty}(\Omega_c))}$. Proving these estimates (the first one in (3.6) and the first and second one in (3.7)) for $k_1 = k_2 = k$ is a standard exercise. Proving $k_1 = k+1$ for the second term in (3.6) and $k_2 = k$ for the third term in (3.7) is not trivial and is far beyond the scope of the present paper. If all the possible regularity is at hand, we should expect $k_1 = k+1$ and $k_2 = k$.

We also define an interpolation operator for scalar potentials. For all $\phi \in \mathscr{C}^1(0,T;\mathbf{H}^1(\Omega_v))$ we define $\pi_h\phi \in \mathscr{C}^1(0,T;\mathbf{X}_h^\phi)$ so that for all $\psi \in \mathbf{X}_h^\phi$ and for a.e. $t \in (0,T)$,

$$(\mu^v\nabla\pi_h\phi, \nabla\psi)_{\Omega_v} = (\mu^v\nabla\phi, \nabla\psi)_{\Omega_v}. \tag{3.8}$$

Likewise, we assume that the following error estimates hold: There is $\ell > 0$ such that

$$\|\nabla(\pi_h\phi - \phi)\|_{L^\infty(0,T;\mathbf{L}^2(\Omega_v))} + \|\nabla(\pi_h\phi - \phi)\times\mathbf{n}^c\|_{L^2(0,T;\mathbf{L}^2(\Sigma))} \leqslant ch^\ell\|\phi\|_{\mathrm{Ho}}. \tag{3.9}$$

When maximal regularity is at hand, it is a standard exercise to prove $\ell = k'$ for the first term in the left-hand side. Proving $\ell = k'$ for the second term is far more technical and relies on $W^{1,\infty}$ estimates.

We finally assume that the algorithm is initialized so that

$$\|\mathbf{H}_0 - \mathbf{H}_{0,h}^c\|_{\mathbf{L}^2(\Omega_c)} \leqslant ch^{k_1}\|\mathbf{H}^c\|_{\mathbf{Ho}}, \quad \|\phi_0 - \phi_0 - \phi_{0,h}\|_{\mathbf{L}^2(\Omega_v)} \leqslant ch^\ell\|\phi\|_{\mathrm{Ho}}. \tag{3.10}$$

Having introduced k_1, k_2, and ℓ, we are now in measure to state the convergence result.

Theorem 3.1. *Under the above assumptions and provided the solution to (2.11) is smooth enough (say* $\|\mathbf{H}^c\|_{\mathbf{Ho}}$ *and* $\|\phi\|_{Ho}$ *finite) and* β *is large enough, the solution to (3.3) satisfies the following error estimates*

$$\|\mathbf{H}^c - \mathbf{H}_h^c\|_{L^\infty(0,T;\mathbf{L}^2(\Omega_c))} + \|\phi - \phi_h\|_{L^\infty(0,T;H^1(\Omega_v))} \leqslant ch^{\min(k_1-\frac{1}{2},k_2+\frac{1}{2},\ell-\frac{1}{2})}, \tag{3.11}$$

$$\|\nabla\times(\mathbf{H}^c - \mathbf{H}_h^c)\|_{L^2(0,T;\mathbf{L}^2(\Omega_c))} + \|\nabla\cdot\mathbf{H}_h^c\|_{L^2(0,T;\mathbf{L}^2(\Omega_c))} \leqslant ch^{\min(k_1-\frac{1}{2},k_2,\ell-\frac{1}{2})}. \tag{3.12}$$

Proof.

(1) We are going to compare the pair $(\mathbf{H}_h^c, \phi_h)$ with $(\pi_h\mathbf{H}^c, \pi_h\phi)$. Define $\mathbf{e}_h = \pi_h\mathbf{H}^c - \mathbf{H}_h^c$, $\epsilon_h = \pi_h\phi - \phi_h$, $\mathbf{d} = \boldsymbol{\pi}_h\mathbf{H}^c - \mathbf{H}^c$, and $\delta = \pi_h\phi - \phi$. Owing to the definition of $\pi_h\mathbf{H}^c$ and $\pi_h\phi$, the following holds

$$(\mu^c\partial_t\mathbf{e}_h, \mathbf{b})_{\Omega_c} + (\mu^v\partial_t\nabla\epsilon_h, \nabla\psi)_{\Omega_v} + a_h((\mathbf{e}_h,\epsilon_h),(\mathbf{b},\psi)) = R((\mathbf{e}_h,\epsilon_h),(\mathbf{b},\psi)),$$

for all $(\mathbf{b},\psi)\in\mathbf{X}_h$ and $t\in(0,T)$, and R is defined by

$$R((\mathbf{e}_h,\epsilon_h),(\mathbf{b},\psi)) = -(\mathbf{u}\times\mu^c\mathbf{d}, \nabla\times\mathbf{b})_{\Omega_c} + \left(\frac{1}{\sigma}\nabla\times\mathbf{d} - \mathbf{u}\times\mu^c\mathbf{d} + \frac{\beta}{h}(\mathbf{d}\times\mathbf{n}^c + \nabla\delta\times\mathbf{n}^v), \mathbf{b}\times\mathbf{n}^c + \nabla\psi\times\mathbf{n}^v\right)_\Sigma.$$

(2) Testing the above equation with the pair $(\mathbf{e}_h,\epsilon_h)$ yields

$$\frac{1}{2}d_t(\mu^c\|\mathbf{e}_h\|^2_{\mathbf{L}^2(\Omega_c)}) + \frac{1}{2}d_t(\mu^v\|\nabla\epsilon_h\|^2_{L^2(\Omega_v)}) + a_h((\mathbf{e}_h,\epsilon_h),(\mathbf{e}_h,\epsilon_h)) = R((\mathbf{e}_h,\epsilon_h),(\mathbf{e}_h,\epsilon_h)).$$

Using a slight variation of Lemma 2.1 gives

$$\begin{aligned} a_h((\mathbf{e}_h,\epsilon_h),(\mathbf{e}_h,\epsilon_h)) \geqslant{}& \frac{1}{2\sigma_1}\|\nabla\times\mathbf{e}_h\|^2_{\mathbf{L}^2(\Omega_c)} + \alpha_0\|\nabla\cdot\mathbf{e}_h\|^2_{\mathbf{L}^2(\Omega_c)} + \frac{\beta}{h}\|\mathbf{e}_h\times\mathbf{n}^c + \nabla\epsilon_h\times\mathbf{n}^v\|^2_{\mathbf{L}^2(\Sigma)} \\ &- \frac{\sigma_1}{2}\|\mathbf{u}\|^2_{\mathbf{L}^\infty(\Omega_c)}\|\mu^c\|^2_{L^\infty(\Omega_c)}\|\mathbf{e}_h\|^2_{\mathbf{L}^2(\Omega_c)} \\ &- \left(\frac{1}{\sigma_0}\|\nabla\times\mathbf{e}_h\|_{\mathbf{L}^2(\Sigma)} + \|\mathbf{u}\|_{\mathbf{L}^\infty(\Omega_c)}\|\mu^c\|_{L^\infty(\Omega_c)}\|\mathbf{e}_h\|_{\mathbf{L}^2(\Sigma)}\right)\|\mathbf{e}_h\times\mathbf{n}^c + \nabla\epsilon_h\times\mathbf{n}^v\|_{\mathbf{L}^2(\Sigma)}. \end{aligned}$$

We now use the inverse inequality $\|\mathbf{b}_h\|_{\mathbf{L}^2(\Sigma)} \leqslant c_i h^{-1/2}\|\mathbf{b}_h\|_{\mathbf{L}^2(\Omega_c)}$ to deduce

$$\begin{aligned} a_h((\mathbf{e}_h,\epsilon_h),(\mathbf{e}_h,\epsilon_h)) \geqslant{}& \left(\frac{1}{2\sigma_1} - \frac{2c_i^2}{\beta\sigma_0^2}\right)\|\nabla\times\mathbf{e}_h\|^2_{\mathbf{L}^2(\Omega_c)} + \alpha_0\|\nabla\cdot\mathbf{e}_h\|^2_{\mathbf{L}^2(\Omega_c)} + \frac{\beta}{h}\left(1-\frac{1}{4}\right)\|\mathbf{e}_h\times\mathbf{n}^c + \nabla\epsilon_h\times\mathbf{n}^v\|^2_{\mathbf{L}^2(\Sigma)} \\ &- c(\mathbf{u},\mu^c,\beta,c_i)\|\mathbf{e}_h\|^2_{\mathbf{L}^2(\Omega_c)}, \end{aligned}$$

and we henceforth assume that β is chosen so that $\beta \geqslant 8c_i^2\sigma_1/\sigma_0^2$ which yields $(\frac{1}{2\sigma_1} - \frac{2c_i^2}{\beta\sigma_0^2}) \geqslant \frac{1}{4\sigma_1}$.
We now bound the residual R from above as follows:

$$\begin{aligned} |R((\mathbf{e}_h,\epsilon_h),(\mathbf{e}_h,\epsilon_h))| \leqslant{}& \frac{1}{8\sigma_1}\|\nabla\times\mathbf{e}_h\|^2_{\mathbf{L}^2(\Omega)} + \frac{\beta}{4h}\|\mathbf{e}_h\times\mathbf{n}^c + \nabla\epsilon_h\times\mathbf{n}^v\|^2_{\mathbf{L}^2(\Sigma)} \\ &+ c\left(h(\|\nabla\times\mathbf{d}\times\mathbf{n}^c\|^2_{\mathbf{L}^2(\Sigma)} + \|\mathbf{d}\|^2_{\mathbf{L}^2(\Sigma)}) + \frac{1}{h}\|\mathbf{d}\times\mathbf{n}^c + \nabla\delta\times\mathbf{n}^v\|^2_{\mathbf{L}^2(\Sigma)} + \|\mathbf{d}\|^2_{\mathbf{L}^2(\Omega)}\right). \end{aligned}$$

Using the interpolation results (3.6), (3.7), (3.9) we infer

$$|R((\mathbf{e}_h,\epsilon_h),(\mathbf{e}_h,\epsilon_h))| \leqslant \frac{1}{8\sigma_1}\|\nabla\times\mathbf{e}_h\|^2_{\mathbf{L}^2(\Omega)} + \frac{\beta}{4h}\|\mathbf{e}_h\times\mathbf{n}^c + \nabla\epsilon_h\times\mathbf{n}^v\|^2_{\mathbf{L}^2(\Sigma)} + r(t)^2,$$

where $\|r\|_{L^2(0,T)} \leqslant ch^{\min(k_1-\frac{1}{2},k_2+\frac{1}{2},\ell-\frac{1}{2})}$.

(3) By combining the lower bound on a_h and the bound on R, one obtains

$$\begin{aligned} &\frac{\mu^c}{2}d_t(\|_h\mathbf{e}_h\|^2_{\mathbf{L}^2(\Omega_c)}) + \frac{\mu^v}{2}d_t(\|\nabla\epsilon_h\|^2_{L^2(\Omega_v)}) + \frac{1}{8\sigma_1}\|\nabla\times\mathbf{e}_h\|^2_{\mathbf{L}^2(\Omega_c)} + \alpha_0\|\nabla\cdot\mathbf{e}_h\|^2_{\mathbf{L}^2(\Omega_c)}\frac{\beta}{2h}\|\mathbf{e}_h\times\mathbf{n}^c + \nabla\epsilon_h\times\mathbf{n}^v\|^2_{\mathbf{L}^2(\Sigma)} \\ &\quad\leqslant c_1\|\mathbf{e}_h\|^2_{\mathbf{L}^2(\Omega_c)} + c_2 r(t)^2. \end{aligned}$$

Using the Gronwall lemma, we infer that for all $t \in (0,T)$

$$\|\mathbf{e}_h\|^2_{\mathbf{L}^2(\Omega_c)} + \|\nabla\epsilon_h\|^2_{L^2(\Omega_v)} + \int_0^t (\|\nabla\times\mathbf{e}_h\|^2_{\mathbf{L}^2(\Omega_c)} + \|\nabla\cdot\mathbf{e}_h\|^2_{\mathbf{L}^2(\Omega_c)}) \leqslant c_2 h^{2\min(k_1-\frac{1}{2},k_2+\frac{1}{2},\ell-\frac{1}{2})} + \|\mathbf{e}_h|_{t=0}\|^2_{\mathbf{L}^2(\Omega_c)} + \|\nabla\epsilon_h|_{t=0}\|^2_{L^2(\Omega_c)}.$$

Using (3.10) together with (3.6), (3.9), and the triangle inequality implies that $\|\mathbf{e}_h|_{t=0}\|_{\mathbf{L}^2(\Omega_c)} + \|\nabla\epsilon_h|_{t=0}\|_{L^2(\Omega_c)}$ is of order $h^{\min(k_1,\ell)}$

Then, using the above result along with the triangle inequality implies

$$\|\mathbf{H}^c - \mathbf{H}^c_h\|_{\mathbf{L}^2(\Omega_c)} \leqslant \|\mathbf{e}_h\|\mathbf{L}^2(\Omega_c) + \|\mathbf{d}\|_{\mathbf{L}^2(\Omega_c)} \leqslant c_2 h^{\min(k_1-\frac{1}{2},k_2+\frac{1}{2},\ell-\frac{1}{2})}.$$

Proceed similarly for the other estimates. □

If full regularity is at hand $k_1 = k+1$, $k_2 = k$, and $\ell = k'$, The above result yields $\|\mathbf{H}^c - \mathbf{H}^c_h\|_{\mathbf{L}^2(\Omega_c)} \leqslant ch^{\min(k+\frac{1}{2},k'-\frac{1}{2})}$. This in turn shows that to obtain optimality we should take

$$k' = k+1, \tag{3.13}$$

i.e., the finite elements used to approximate the scalar potential are one degree higher than those used to approximate the magnetic filed in Ω_c. This is coherent with the fact that the magnetic field in Ω_v is the gradient of ϕ, i.e., the magnetic field is deduced from ϕ by derivation. In conclusion, if we set $k' = k+1$ and if full regularity is guaranteed, the above theorem yields

$$\|\mathbf{H}^c - \mathbf{H}^c_h\|_{L^\infty(0,T;\mathbf{L}^2(\Omega_c))} + \|\phi - \phi_h\|_{L^\infty(0,T;H^1(\Omega_v))} \leqslant ch^{k+\frac{1}{2}} \tag{3.14}$$

$$\|\nabla\times(\mathbf{H}^c - \mathbf{H}^c_h)\|_{L^2(0,T;\mathbf{L}^2(\Omega_c))} + \|\nabla\cdot\mathbf{H}^c_h\|_{L^2(0,T;\mathbf{L}^2(\Omega_c))} \leqslant ch^k. \tag{3.15}$$

These estimates are confirmed by the numerical tests reported in Section 4.

4. Convergence tests

In this section, we give technical implementation details and we report convergence tests that illustrate the capability of the approximation technique introduced in the previous section. We limit the convergence tests to magnetodynamic examples since the velocity field is inessential in the convergence analysis.

4.1. Implementation details

We henceforth assume that the domains Ω_c and Ω_v are either two-dimensional or axisymmetric. In the axisymmetric situation we use finite elements in the meridian plane and Fourier expansions in the azimuthal direction. For instance, the approximate scalar potential is decomposed as follows:

$$\phi_h(r,\theta,z,t) = \phi^c_{h,0}(r,z,t) + \sum_{m=1}^{M} \phi^c_{h,m}(r,z,t)\cos(m\theta) + \phi^s_{h,m}(r,z,t)\sin(m\theta),$$

where $\phi^c_{h,0}$, $\phi^c_{h,m}$, and $\phi^s_{h,m}$ are time-dependent two-dimensional finite element functions. The same decomposition is used for each component of the approximate magnetic field. Depending on the situation $\mathbb{P}_1$ (piecewise linear) or $\mathbb{P}_2$ (piecewise quadratic) finite elements are used for $\mathbf{H}^c$, but $\mathbb{P}_2$ elements are always used for the scalar potential ϕ. The finite element meshes are composed of triangles and are constructed using a Delaunay mesh generator [24]. The notation h that is used hereafter denotes the typical mesh size of meshes. The number of triangles in meshes of typical meshsize h is roughly $\mathcal{O}(h^{-2})$.

The time is approximated by using the backward difference formula of second-order (BDF2). The analysis of the fully discretized method goes along the same line as that of the semi-discretized method and the same estimates as those in (3.11), (3.12) can be obtained but for a Δt^2 additional term in the right-hand sides. We omit the details for brevity. The fully discretized problem yields two linear systems for each Fourier mode at

each time step. The linear systems are preconditioned by sparse, thresholded, incomplete LU factorization and are solved using the version of BiCG-stab which is implemented in the package splib [7].

4.2. Time-independent 2D convergence tests

We show in this section that the method converges as expected by solving a two-dimensional problem. To focus on the approximation capability of the method with respect to space, we solve the following time-independent problem

$$\begin{cases} \mu^c \mathbf{H}^c = -\nabla \times \mathbf{E}^c, & \nabla \times \mathbf{H}^c = \sigma(\mathbf{E}^c + \mathbf{u} \times \mu^c \mathbf{H}^c) + \mathbf{j}^s & \text{in } \Omega_c, \\ \mu^v \nabla \phi = -\nabla \times \mathbf{E}^v, & \nabla \cdot \mathbf{E}^v = 0 & \text{in } \Omega_v, \\ \mathbf{H}^c \times \mathbf{n}^c + \nabla \phi \times \mathbf{n}^v = 0 & \mathbf{E}^c \times \mathbf{n}^c + \mathbf{E}^v \times \mathbf{n}^v = 0 & \text{on } \Sigma, \\ \mathbf{E}^c \times \mathbf{n}^c|_{\Gamma_c} = \mathbf{a} & \mathbf{E}^v \times \mathbf{n}^v|_{\Gamma_v} = \mathbf{a}. & \end{cases} \tag{4.1}$$

Since the presence of the velocity field is inessential in the convergence analysis, we henceforth restrict ourselves in this section to $\mathbf{u} = 0$. We start with a two-dimensional situation, i.e., nothing depends on z. Moreover, we assume that $\mathbf{E}$ points in the z-direction and the z-component of $\mathbf{H}^c$ is zero, i.e., $\mathbf{E} = (0, 0, E_z)$, $\mathbf{H}^c = (H_x, H_y, 0)$. The computational domain is $\Omega = (0,1)^2$ with $\Omega_c = (0, \frac{1}{2}) \times (0, 1)$ and $\Omega_v = (\frac{1}{2}, 1) \times (0, 1)$. The interface between Ω_c and Ω_v is $\Sigma = \{\frac{1}{2}\} \times (0, 1)$. We set $\sigma = 1, \mu^c = \mu$ and $\mu^v = 1$. The exact solution that we pick is

$$\text{in } \Omega_v \begin{cases} E_z = -\cos(x - \frac{1}{2})e^{-y} + x^2 - y^2 + 2xy - \frac{1}{4}, \\ \phi = -\sin(x - \frac{1}{2})e^{-y} + 2xy - x^2 + y^2, \end{cases} \tag{4.2}$$

$$\text{in } \Omega_c \begin{cases} E_z = -e^{-y} + (x - \frac{1}{2})^2 + \mu(1 + 2y)(x - \frac{1}{2}) + y - y^2, \\ H_x = \frac{1}{\mu}(-e^{-y} - 1 + 2y) - 2(x - \frac{1}{2}), \\ H_y = \frac{2}{\mu} = \frac{2}{\mu}(x - \frac{1}{2}) + (1 + 2y). \end{cases} \tag{4.3}$$

Then the current is set so that $\mathbf{j}^s = \nabla \times \mathbf{H}^c - \sigma \mathbf{E}$. This solution is designed so that $(\mu H_x - \partial_x \phi)|_\Sigma = 0$ and $(H_y - \partial_y \phi)|_\Sigma = 0$. The normal component of the magnetic field is discontinuous across Σ when $\mu \neq 1$, i.e., $(\mathbf{H}^c - \mathbf{n}^c + \nabla \phi \cdot \mathbf{n}^v)|_\Sigma \neq 0$, but the normal component of the magnetic induction is always continuous $(\mu^c \mathbf{H}^c \cdot \mathbf{n}^c + \mu^v \nabla \phi \cdot \mathbf{n}^v)|_\Sigma = 0$.

The above problem is solved using continuous $\mathbb{P}_1$ elements for $\mathbf{H}^c$ and continuous $\mathbb{P}_2$ elements for ϕ on meshes of meshsize in the range $1/160 \leqslant h \leqslant 1/10$. The results are reported in Fig. 2 for three values of $\mu \in \{0.1, 1, 10\}$. We show in this figure the relative error on $\mathbf{H}^c$ in the L^2-norm, i.e., $\|\mathbf{H}^c - \mathbf{H}_h^c\|_{L^2}$, and in the $\mathbf{H}_{\text{curl}}$-norm, i.e., $(\|\mathbf{H}^c - \mathbf{H}_h^c\|_{L^2}^2 + \|\nabla \times (\mathbf{H}^c - \mathbf{H}_h^c)\|_{L^2}^2)^{\frac{1}{2}}$. We also show in the figure the L^2-norm of $\nabla \cdot \mathbf{H}_h^c$ and the error on the scalar potential in the non-conducting medium measured in the H^1-norm. All these errors are normalized by the corresponding norm of the exact solution. For the three values of μ tested, the error measured on $\mathbf{H}^c$ in the L^2-norm behaves like $\mathcal{O}(h^{\frac{3}{2}})$ and when measured in the $\mathbf{H}_{\text{curl}}$-norm it behaves like $\mathcal{O}(h)$. The error on the divergence of the magnetic field is also $\mathcal{O}(h)$. The rate of convergence on ϕ in the H^1-norm is $\mathcal{O}(h^{\frac{3}{2}})$. All these rates confirm the theoretical estimates (3.14), (3.15) (note that the error analysis for the time-dependent problem is almost identical to that of the time-independent problem and yields the same error estimates. The details are omitted for brevity).

4.3. Time-independent 3D convergence tests

We still consider the time-independent problem (4.1) in this section but we now consider a three-dimensional situation. The domain is a torus of square cross section of side 4 and of radius 3. Using cylindrical coordinates (r, θ, z), the exact definition of the computational domain is

$$\Omega = \{(r, \theta, z); 1 \leqslant r \leqslant 5; -2 \leqslant z \leqslant 2; \theta \in [0, 2\pi)\}, \tag{4.4}$$

$$\Omega_c = \{(r, \theta, z); ((r - 3)^2 + z^2)^{\frac{1}{2}} \leqslant 1; \theta \in [0, 2\pi)\}, \tag{4.5}$$

$$\Omega_v = \Omega \setminus \Omega_v. \tag{4.6}$$

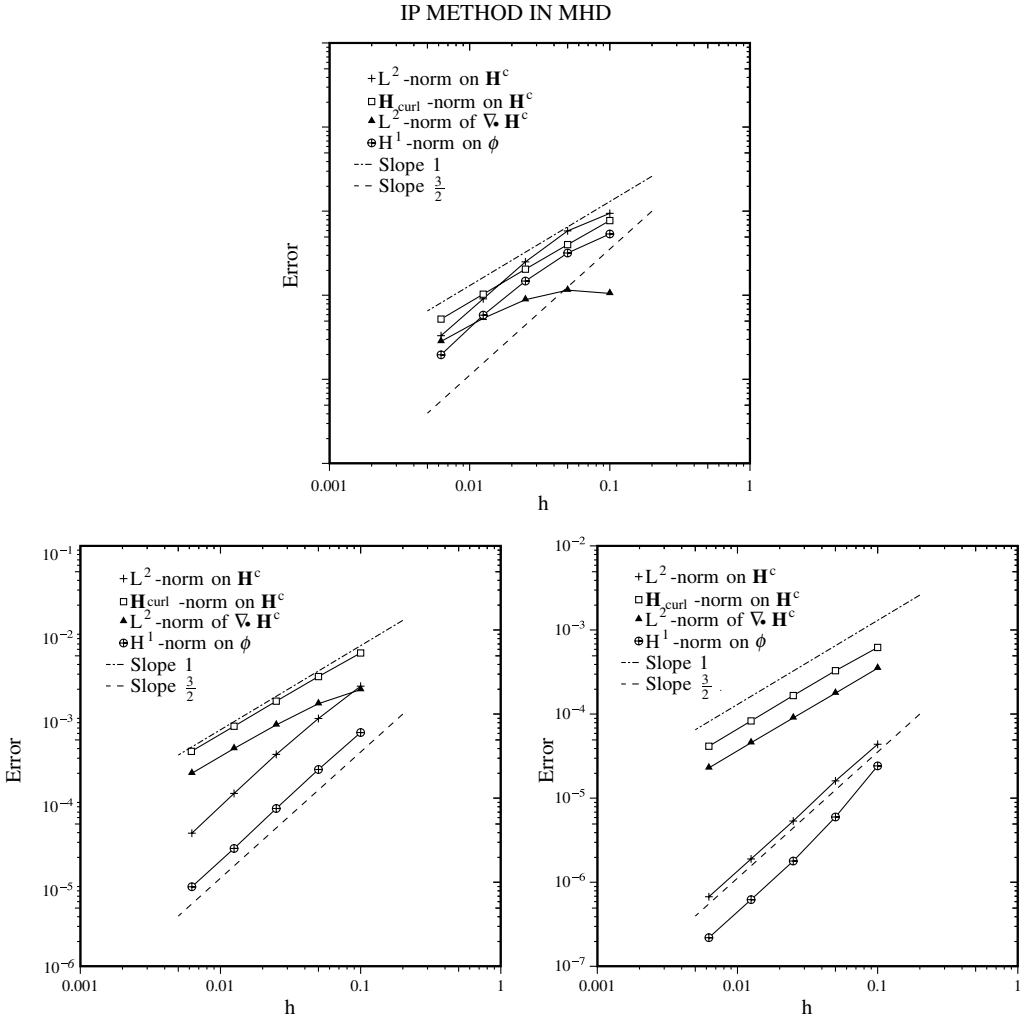

Fig. 2. Time-independent two-dimensional convergence tests: top $\mu = 0.1$; bottom left $\mu = 1$; bottom right $\mu = 10$. Norms $\|\mathbf{H}_h^c - \mathbf{H}^c\|_{\mathbf{L}^2}/\|\mathbf{H}^c\|_{\mathbf{L}^2}$, $\|\nabla \times (\mathbf{H}_h^c - \mathbf{H}^c)\|_{\mathbf{L}^2}/\|\mathbf{H}^c\|_{\mathbf{L}^2}$, $\|\nabla \cdot \mathbf{H}_h^c\|_{\mathbf{L}^2}\|\mathbf{H}^c\|_{\mathbf{L}^2}$, and $\|\phi_h - \phi\|_{H^1}/\|\phi\|_{\mathbf{L}^2}$ as functions of the mesh-size h in log scales.

We set the boundary data and the current so that the exact solution is

$$\text{in } \Omega_{\mathrm{v}} \begin{cases} E_r = 0, \\ E_\theta = -(\frac{1}{3}r^2 + 1)(\cos\theta + \sin\theta), \\ E_z = z(r - r^{-1})(\cos\theta - \sin\theta), \\ \phi = z(r + r^{-1})(\cos\theta + \sin\theta), \end{cases} \tag{4.7}$$

$$\text{in } \Omega_{\mathrm{c}} \begin{cases} H_r = z(1 - r^{-2})(\cos\theta + \sin\theta), \\ H_\theta = z(1 + r^{-2})(\cos\theta - \sin\theta), \\ H_z = (r + r^{-1})(\cos\theta + \sin\theta), \end{cases} \tag{4.8}$$

and the magnetic permeabilities are $\mu^c = \mu^v = 1$ and we set $\sigma = 1$. We make convergence tests with respect to the meshsize using meshes with relative meshsize $\frac{1}{160} \leqslant \frac{h}{4} \leqslant \frac{1}{10}$ (recall the width of the square cross section is 4). The results are reported in Fig. 3. As in the two-dimensional case we observe $\mathcal{O}(h^{\frac{3}{2}})$ convergence on the magnetic field in the L^2-norm and $\mathcal{O}(h)$ convergence in the $\mathbf{H}_{\mathrm{curl}}$-norm. The divergence of $\mathbf{H}^c$ converges like $\mathcal{O}(h)$ in the L^2-norm.

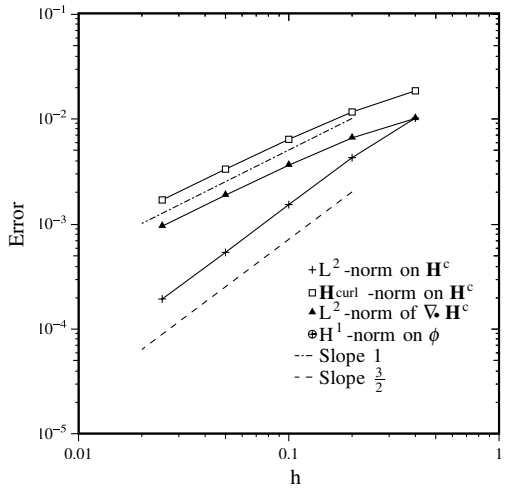

Fig. 3. Three-dimensional steady problem: norms $\|\mathbf{H}_h^c - \mathbf{H}^c\|_{\mathbf{L}^2}/\|\mathbf{H}^c\|_{\mathbf{L}^2}$, $\|\nabla \times (\mathbf{H}_h^c - \mathbf{H}^c)\|_{\mathbf{L}^2}/\mathbf{H}^c\|_{\mathbf{L}^2}$, and $\|\nabla \cdot \mathbf{H}_h^c\|_{\mathbf{L}^2}/\mathbf{H}^c\|_{\mathbf{L}^2}$ as functions of the mesh-size h in log scales.

4.4. Convergence tests on a 3D time-dependent problem

We finish this section by reporting convergence tests on the three-dimensional time-dependent problem.

The domain is the torus defined by (4.4)–(4.6). The boundary data and the current are set so that the exact solution is

$$\text{in } \Omega_v \begin{cases} E_r = 0, \\ E_\theta = (\frac{1}{3}r^2 + 1)(\cos\theta + \sin\theta)\sin(t), \\ E_z = -z(r - r^{-1})(\cos\theta - \sin\theta)\sin(t), \\ \phi = z(r + r^{-1})(\cos\theta + \sin\theta)\cos(t), \end{cases} \tag{4.9}$$

$$\text{in } \Omega_c \begin{cases} H_r = z(1 - r^{-2})(\cos\theta + \sin\theta)\cos(t), \\ H_\theta = z(1 + r^{-2})(\cos\theta - \sin\theta)\cot(t), \\ H_z = (r + r^{-1})(\cos\theta + \sin\theta)\cos(t). \end{cases} \tag{4.10}$$

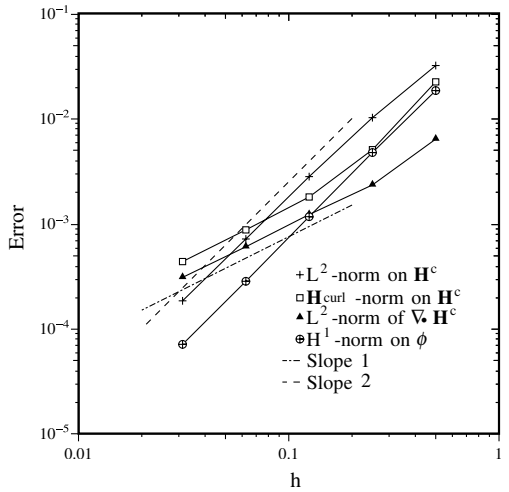

Fig. 4. Three-dimensional time-dependent problem: norms $\|\mathbf{H}_h^c - \mathbf{H}^c\|_{\mathbf{L}^2}/\mathbf{H}^c\|_{\mathbf{L}^2}$, $\|\nabla \times (\mathbf{H}_h^c - \mathbf{H}^c)\|_{\mathbf{L}^2}/\|\mathbf{H}^c\|_{\mathbf{L}^2}$, $\|\nabla \cdot \mathbf{H}_h^c\|\mathbf{L}^2/\|\mathbf{H}^c$, and $\|\phi_h - \phi\|_{H^1}/\|\phi\|_{L^2}$ at time $T = 2$ as functions of the mesh-size h in log scales.

The magnetic permeability and conductivity are $\mu^c = \mu^v = 1$, $\sigma = 1$.

We make convergence tests with respect to the meshsize using meshes with relative meshsize $\frac{1}{128} \leqslant \frac{h}{4} \leqslant \frac{1}{8}$. The time step $\Delta t = 2 \times 10^{-3}$ is chosen to be small enough so that the time approximation error is negligible compared to that induced by the space approximation.

The results are reported in Fig. 4. The figure shows $\|\mathbf{H}_h^c - \mathbf{H}^c\|_{\mathbf{L}^2}/\|\mathbf{H}^c\|_{\mathbf{L}^2}$, $\|\nabla \times (\mathbf{H}_h^c - \mathbf{H}^c)\|_{\mathbf{L}^2}/\|\mathbf{H}^c\|_{\mathbf{L}^2}$, $\|\nabla \cdot \mathbf{H}_h^c\|_{\mathbf{L}^2}/\|\mathbf{H}^c\|_{\mathbf{L}^2}$ and $\|\phi_h - \phi\|_{H^1}/\|\phi\|_{L^2}$ at time $T = 2$. We observe $\mathcal{O}(h^2)$ convergence on the magnetic field in the L^2-norm both in Ω_c and Ω_v. The curl of $\mathbf{H}_h^c$ is $\mathcal{O}(h)$ accurate in the L^2-norm. The divergence of $\mathbf{H}_h^c$ converges to zero like $\mathcal{O}(h)$ in the L^2-norm. We observe that these results are compatible with the theoretical error estimates (3.11), (3.12). The estimates on the L^2-norm of the magnetic field seems to be slightly super-convergent by $\mathcal{O}(h^{\frac{1}{2}})$.

5. Applications

We report in this section tests that we made to validate our code in three dimensions. In this entire section μ is assumed to be constant and $\mu^c = \mu^v$. All the computations reported have been done using $\mathbb{P}_1$ finite elements in the conducting region and $\mathbb{P}_2$ finite elements in the non-conducting region.

5.1. Ohmic decay in a compact conducting domain

We set the velocity field to zero and we assume that μ and σ are constants. The MHD equations (2.5) then reduce to the vector heat equation in the conducting region for $\mathbf{H}^c$ and to the Laplace equation in the non-conducting region for the scalar potential:

$$\begin{cases} \partial_t \mathbf{H}^c = \Delta \mathbf{H}^c & \text{in } \Omega_c, \\ \Delta \partial_t \phi = 0 & \text{in } \Omega_v, \ \ \phi \to 0 \text{ at infinity}, \\ \mathbf{H}^c|_\Sigma = \nabla \phi|_\Sigma, \quad \mathbf{H}^c|_{t=0} = \mathbf{H}_0, \quad \phi|_{t=0} = \phi_0. \end{cases} \tag{5.1}$$

In the above equations, space and time have been non-dimensionalized using a reference length-scale L and the diffusive time scale $T_d = \mu\sigma L^2$. Searching for an exponentially decaying solution, $H^c = H_0^c = \mathbf{H}_0^c e^{\gamma t}$, leads to an eigenvalue problem. Analytic solutions to this eigenvalue problem are known only for some simple geometries of the conducting domain. In the following, we denote by γ the smallest (obviously real) corresponding eigenvalue.

In this section we consider two types of conducting solids: a sphere and ellipsoids (prolate and oblate).

5.1.1. Ohmic decay in a sphere

We consider a sphere of radius $R = 1$ (i.e., the radius of the sphere is the reference length scale). The ohmic decay in a sphere is a textbook diffusion problem [22]. The theoretical decay-rate is $|\gamma_{\text{th}}| = \pi^2$ The corresponding scalar potential in the non-conducting medium in cylindrical coordinates is the dipole field $\phi = -z\rho^{-3} J_{3/2}(\pi) \mathrm{e}^{-|\gamma_{\text{th}}|t}$ where $\rho = (r^2 + z^2)^{1/2}$ (the dipole moment being aligned with the z-axis). The corresponding magnetic field in cylindrical coordinates is given by

$$H_r = \sin(\varphi) B_\rho + \cos(\varphi) B_\varphi, \tag{5.2}$$

$$H_z = \cos(\varphi) B_\rho - \sin(\varphi) B_\varphi, \tag{5.3}$$

where $\cos(\varphi) = z/\rho$, $\sin(\varphi) = r/\rho$, and

$$B_\rho = 2\mathrm{e}^{-|\gamma_{\text{th}}|t} \cos(\varphi) J_{3/2}(\pi\rho) \rho^{-3/2}, \tag{5.4}$$

$$B_\varphi = \mathrm{e}^{-|\gamma_{\text{th}}|t} \sin(\varphi) (J_{3/2}(\pi\rho) - \pi\rho J_{1/2}(\pi\rho)) \rho^{-3/2}. \tag{5.5}$$

The above field is used as the initial condition in our tests. The outer boundary of the non-conducting medium is the sphere of radius $R_v = 10$. We use meshes with meshsizes $h = 1/10$, $1/40$, $1/80$ to observe the convergence with respect to the spatial resolution. The time step is taken to be $\Delta t = 10^{-3}$.

The time evolution of the magnetic energy and its instantaneous decay rate are shown in Fig. 5. More precisely, upon setting $E_{\text{mag}} = \frac{1}{2}\int_{\Omega_c} \|\mathbf{H}^c\|^2$, we report E_{mag} as a function of time t in Fig. 5a and $\mathrm{d}\log(E_{\text{mag}})/\mathrm{d}t$ in Fig. 5b. The decay rate reaches a plateau after a few time-steps for the three resolutions considered. The value of the plateau γ is recorded and its absolute value is reported in Table 1.

Note that after 8–10 Ohmic decay times ($\sim T_d/|\gamma|$), the computed decay rate increases and finally tends to zero. This is a consequence of problem (5.1) not being well-posed at steady state. As a result, at steady state we obtain a magnetic field whose amplitude is controlled by the divergence of the initial field. Since we use Lagrange interpolants to initialize our computations, the divergence of our initial data is of order $h^{k'} = h^2$. This leads to a non-dissipative magnetic energy at steady state. This residual magnetic energy, denoted by E_{noise}, is reported in Table 1. Observe that E_{noise} goes to zero as $h^{3.4} \to 0$.

5.1.2. Ohmic decay in an ellipsoid

In order to measure the influence of the conductor geometry, we now study the ohmic decay in ellipsoids. Recall that no analytical expression of the decay-rate is available in this case. Let us denote by a, b, c the semi-axes, with $a = b$ to enforce axisymmetry. We refer to a and c as the half-width and the half-height, respectively. Letting V be the volume of the ellipsoid, the reference lengthscale is defined to satisfy $\frac{4}{3}\pi L^3 = V$, i.e., L is the radius of the sphere having the same volume. Two cases are considered in detail: (1) an 'oblate' spheroid $a = 2$ and $c = 0.25$ and (2) a 'prolate' spheroid $a = 0.75$ and $c = 1.78$. Each ellipsoid is embedded in a non-conducting sphere of radius $R_v = 10$.

The initial magnetic field is chosen to be uniform and parallel to the z-axis. The corresponding magnetic potential in vacuum is $\phi = z$. After $t = 0$, this field is gradually extinguished at Γ_v by enforcing:

$$\phi(t)|_{\Gamma_v} = \frac{z}{1 + (t/t_{\text{ext}})^3},$$

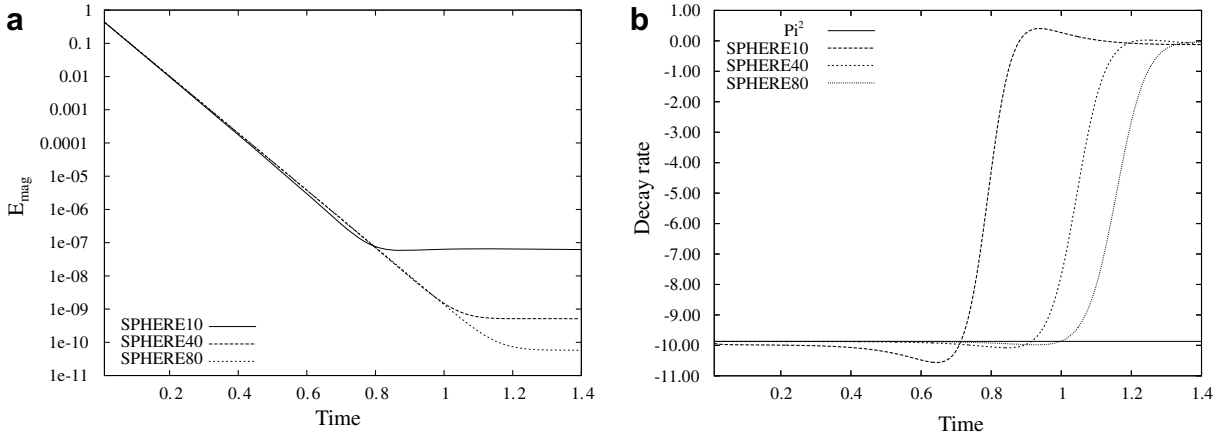

Fig. 5. Ohmic diffusion in a sphere for different mesh sizes $h = 1/10, 1/40, 1/80$: time evolution of (a) magnetic energy and (b) decay rate of the magnetic energy.

Table 1
Ohmic diffusion in a sphere

h	$\lvert\gamma\rvert$	Error (%)	t_{noise}	E_{noise}	$np(H)$	$np(\phi)$
1/10	9.9921	1.2	0.65	0.62×10^{-7}	228	403
1/40	9.8741	0.05	0.9	0.51×10^{-9}	3358	6508
1/80	9.8686	0.01	1	0.51×10^{-10}	13,182	25,572

h is the mesh size; $|\gamma|$ is the decay rate of the magnetic energy; "error" is the quantity $|-\pi^2 - |\gamma||/\pi^2$; t_{noise} is the characteristic time when the exponential decay ends; E_{noise} is the residual magnetic energy; $np(H)$ is the number of $\mathbb{P}_1$ nodes for the magnetic field in Ω_c; $np(\phi)$ is the number of $\mathbb{P}_2$ nodes for the magnetic potential in Ω_v.

where t_{ext} is the extinction time. Since we expect the decay rate to be of the same order as that of the sphere ($|\gamma_{th}| \sim \pi^2$), we set $t_{ext} = 10^{-2}$ and $\Delta t = 5 \times 10^{-4}$. This choice guarantees that t_{ext} is significantly smaller than the ohmic diffusion time.

The instantaneous decay-rates of the radial and vertical components of the magnetic field are displayed in Fig. 6 for the two ellipsoids and two meshsizes ($h = 1/20, 1/40$). After a few time-steps, each decay rate reaches a plateau, then increases and finally tends to zero like in the case of the sphere.

We observe that the decay-rate of the oblate spheroid is about -9.3 and that of the prolate spheroid is about -13.4. In other words by denoting γ_{obl}, γ_{pro}, and γ_{sph} the decay rates of the oblate ellipsoid, the prolate ellipsoid, and the sphere, we have

$$|\gamma_{obl}| < |\gamma_{sph}| < |\gamma_{pro}|.$$

We interpret this result as follows. Since in the sphere the decaying magnetic field is supported by an azimuthal current density that is maximum at $r \simeq 0.9R$, it seems natural that oblateness allows for a larger effective radius for the current and consequently a longer decay time as long as the corresponding reduction of the half-height c does not constrain too much the total current. In conclusion, the absolute value of the decay rate decreases then increases as a goes from 0 to $+\infty$ as shown in Fig. 7 i.e., there exists an oblate ellipsoid for $a = 1.5$ with a decay rate whose absolute value is minimum. This curve suggests that the ohmic decay rate of astro-physical objects flattened by rotation may be different from that of similar undeformed objects.

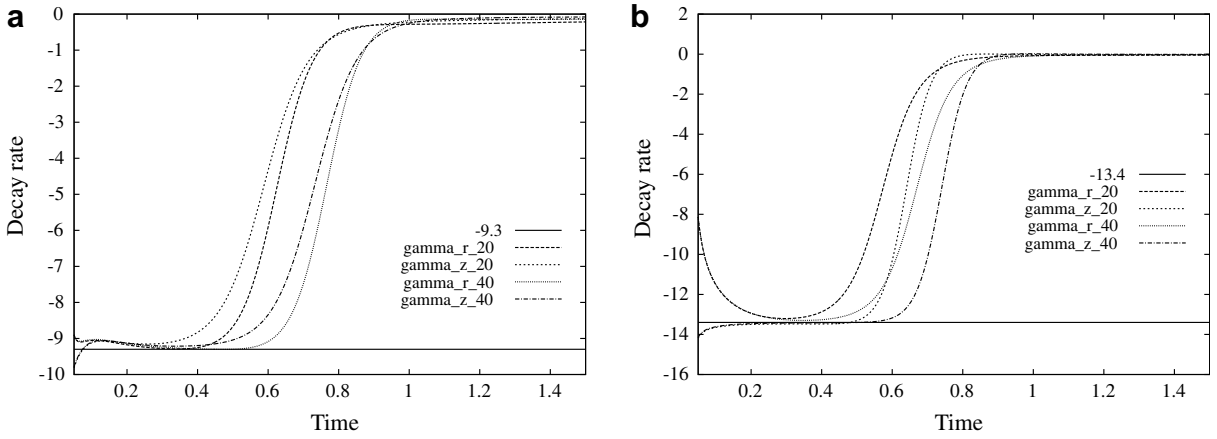

Fig. 6. Ohmic diffusion in two spheroids for different mesh sizes $h = 1/20, 1/40$: time evolution of the decay rates for the H_r component γ_r and the H_z component γ_z: (a) oblate spheroid, (b) prolate spheroid.

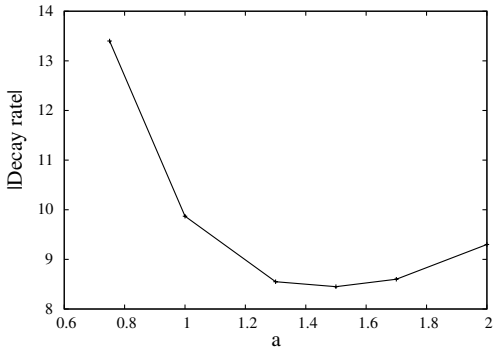

Fig. 7. Absolute value of the decay rate as a function of the half-width of the ellipsoid a. The minimum is reached for $a = 1.5$.

5.2. Kinematic dynamo

We now turn our attention to the dynamo action. For the time being we only consider the kinematic dynamo, i.e., that for which the velocity field is prescribed and time-independent. Validation of the kinematic code is a prerequisite for the full nonlinear dynamo problem, where the Navier–Stokes equations including the Lorentz force are also solved. Henceforth our domain is composed of a solid component of constant conductivity σ_{solid} and a fluid component of constant conductivity σ_{fluid} such that $\sigma_{\text{solid}}/\sigma_{\text{fluid}} = 5$. The problem is described by (2.3) where $\mathbf{u}$ is zero in the solid and $\mathbf{u}$ is prescribed in the fluid. The current $\mathbf{j}^s$ is set to zero everywhere. Letting L be a reference length scale, the time is non-dimensionalized with respect to the diffusive time, $T_d = \mu\sigma_{\text{fluid}}L^2$. Letting U be a reference velocity scale, we define the magnetic Reynolds number $R_m = \mu\sigma_{\text{fluid}}UL$.

The configuration we want to model is inspired from the so-called Perm device [11,13]. This experiment aims at generating the dynamo effect in a strongly time-dependent helical flow created in a toroidal channel after impulsively stopping the fast rotating container. Two axisymmetric conducting media whose meridian sections are shown in Figs. 8a and b are considered. The first case consists of a ring torus (i.e., of circular cross-section) hereafter referred to as 'torus'. The reference length scale is chosen so that the non-dimensional mean radius of the torus (i.e., the distance between the z-axis and the center of the cross section) is $R = 4$. The non-dimensional radius of the circular cross section is $\rho_1 = 1.6$. The inner part of the torus, $0 \leqslant \rho < \rho_0 = 1.2$, is occupied by the conducting fluid and is referred to as the fluid channel. The outer part of the torus, $\rho_0 < \rho < \rho_1$, is occupied by the conducting solid. The second case consists in a variation of the torus geometry where the conducting domain includes flat equatorial protuberances. The second setting is hereafter referred to as the 'Perm' case, since it is closer to the real experimental geometry.

The flow velocity is assumed to have a uniform azimuthal component that we henceforth denote by U_a. The reference velocity U is chosen to be $U = U_a\rho_0$ so that the magnetic Reynolds number can be rewritten as $R_m = \mu\sigma_{\text{fluid}}U_a(\rho_0 L)$. The non-dimensional helical flow in the fluid channel is then defined in cylindrical coordinates by

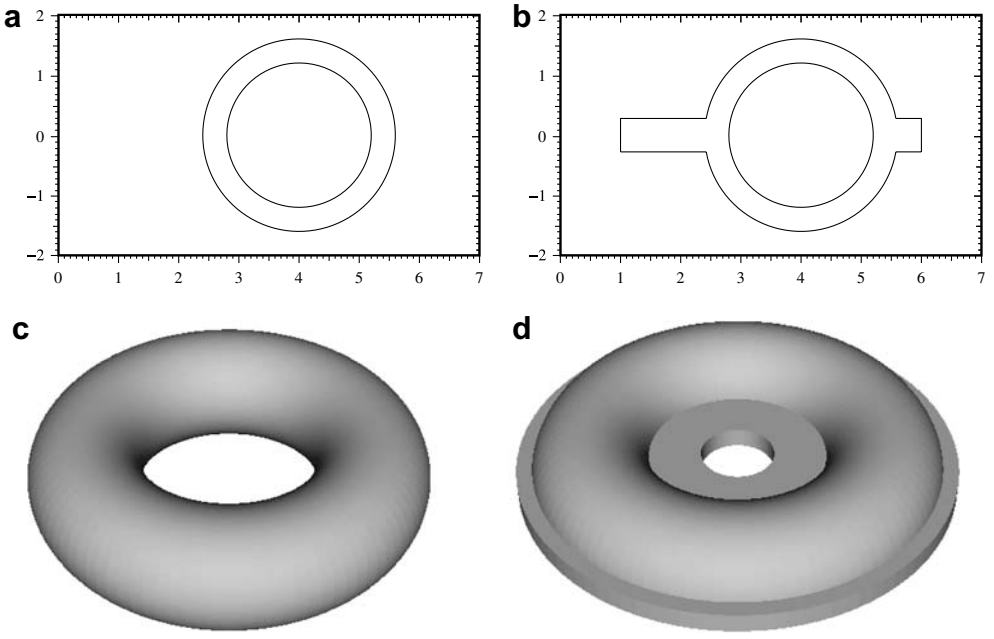

Fig. 8. Schematic representation of the two tori configurations, (a) and (b) are cross-sections in the meridian plane; (c) and (d) are three-dimensional renderings, (a)–(c) correspond to the 'Torus' case and (b)–(d) to the 'Perm' case.

$$\begin{cases} u_r = -\chi \frac{1}{\rho_0} \frac{Rz}{\rho_0 r}, \\ u_\theta = \frac{1}{\rho_0}, \\ u_z = \chi \frac{1}{\rho_0} \frac{R(r-R)}{\rho_0 r}, \end{cases} \tag{5.6}$$

where χ is a constant hereafter referred to as the poloidal to toroidal velocity ratio. We choose $\chi = 1$ as in [11], where the case of the straight cylinder ($R = \infty$) is studied in details. This flow is unphysical since it slips on the shell, but our goal is to mimic the classical steady Ponomarenko flow in the torus geometry. Recall that the Ponomarenko flow is defined in a straight cylinder. This test is meant to compare the thresholds between our curved pipes and the Ponomarenko case. More realistic simulations are currently being done and will be reported elsewhere [19]. Since the flow $\mathbf{u}$ is axisymmetric, the term $\nabla \times (\mathbf{u} \times \mathbf{H}^c)$ cannot transfer energy between the azimuthal modes of $\mathbf{H}^c$, i.e., the azimuthal modes are uncoupled; therefore, the initial magnetic field in the conductor is set to contain all the azimuthal modes that we want to test. To achieve this goal, the simulations are initialized as follows. The magnetic field is set to zero at $t = 0$, then we impose an azimuthal current on the modes $m \in 1, \ldots, 5$ for $0 < t \leqslant t_{\text{ext}} = 0.01$, i.e., after t_{ext} the current is set to zero. We use meshes with meshsize $h = 1/20$ and a time step $\Delta t = 5 \times 10^{-4}$.

The magnetic energy on every mode is recorded as a function of time for various magnetic Reynolds numbers $R_m \in [10, 30]$. Fig. 9a shows the magnetic energy as a function of time for the 'Perm' case at $R_m = 30$. After thorough investigations, we have found that $m = 3$ is the critical mode corresponding to the lowest critical magnetic Reynolds number in both the 'Perm' and the 'Torus' cases. More precisely we have determined $R_m^c(\text{Perm}) \simeq 16 \pm 0.5$ and $R_m^c(\text{torus}) \simeq 17.5 \pm 0.5$ (see Fig. 9b).

The above thresholds are lower than the threshold $R_m^c = 22.8$ found in [11] with the ratio $(\rho_1 - \rho_0)/\rho_0 = 0.33$ in the case of a straight pipe (i.e., a torus with $R/\rho_0 \to \infty$). Curvature effects seem to be solely responsible for this difference, since all cases have an envelope with the same radius and the same fivefold increase of conductivity. We show in Fig. 10 the H_θ-component of the unstable mode for the 'Perm' case at $R_m = 17 > R_m^c(\text{Perm})$. Observe that the support of this unstable eigenmode is localized close to $\rho \approx \rho_0$, i.e., in the region of maximum shear. This eigenmode has a double helix shape and has the same helicity sign as that of the velocity field. By recording the time evolution of the magnetic field at various fixed points in the fluid domain, we observe that each signal is composed of a growing exponential envelope and of a periodic component. At every point, we observe that the period of the periodic component is $T_{\text{period}} \approx 4$ related to the angular frequency $\omega = 2\pi/T_{\text{period}}$. The phase speed associated with an $m = 3$ mode is by definition $\frac{\omega}{3}$.

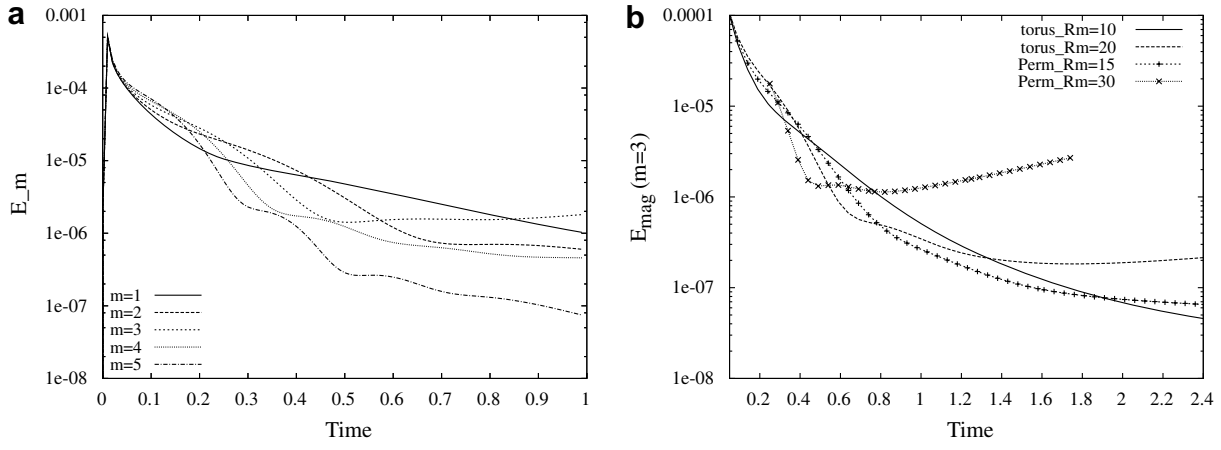

Fig. 9. Time evolution of the magnetic energy: (a) at $R_m = 30$ for m $\in \{1, \ldots, 5\}$ for the Perm case; (b) for $m = 3$ at different R_m for the two cases: 'torus', 'Perm'.

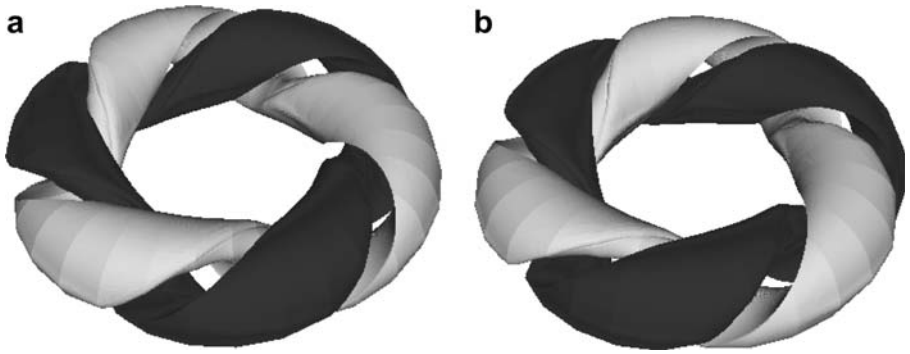

Fig. 10. Perm dynamo at R_m=17: iso-surfaces of the H_θ component of the $m = 3$ mode; $H_\theta = 25\%$ of the minimum value (black) and $H_\theta = 25\%$ of the maximum value (white) at (a) t=1 and (b) $t = 2 \simeq 1 + \frac{1}{4}T_{\text{period}}$, where T_{period} is the period.

By taking two snapshots of the magnetic field at two times t_1, t_2 such that $t_2 - t_1 = \frac{1}{4}T_{\text{period}}$, the angular displacement between these two snapshots should be

$$\frac{\omega}{3}\frac{1}{4}T_{\text{period}} \approx \frac{1}{6}\pi = 30^\circ,$$

which is exactly the angular displacement that is observed in Figs. 10a and b.

In the above discussion we have assumed that the flow is steady. In the Perm experiment, this is definitely not the case since high magnetic Reynolds numbers are generated by impulsively braking the container. Before doing simulations with time-dependent flows, which could be done in principle with our code, it is thus wise to verify that the time interval where R_m stays above critical (estimated from experiments using water models) is indeed larger than the dynamo growth time T_{growth}. Let us consider the growth time at $R_m = 30$, i.e. about twice the critical value. Below $R_m = 30$ we have found that the real part of the growth rate γ is quasi-linear with respect to R_m: $\Re(\gamma) = \alpha(R_m/R_m^c - 1)$ with $\alpha \simeq 2.24$. At R_m=30, the characteristic growth time is thus about $T_{\text{growth}} \approx T_d/(\alpha(30/16 - 1)) \approx 0.51T_d$, which must be compared with the life time of the flow at $R_m \geqslant 30$, which is about 10 rotation periods according to [13], i.e., $T_{\text{flow}} = 10(2\pi R)/U_a$. This leads to the following estimation

$$\frac{T_{\text{flow}}}{T_{\text{growth}}} \approx \frac{20\pi R}{0.5\mu\sigma_{\text{fluid}}L^2U_a} = \frac{2\pi\rho_0 RL^{-1}}{0.5R_m} \approx 20$$

which is hoped to be sufficient for the dynamo action to settle in the Perm experiment. This conjecture however deserves more detailed examination by taking into account the effective time history of the magnetic Reynolds number.

6. Conclusion

The Maxwell equations in the MHD limit in heterogeneous domains are solved by using the magnetic field $\mathbf{H}^c$ in the conducting regions and the magnetic scalar potential ϕ in the non-conducting regions. We use Lagrange finite elements and enforce continuities across interfaces using an interior penalty technique à la Nitsche/Dupont–Baker. The method is shown to be stable and convergent. In axisymmetric domains, finite elements are used in the meridian plane and Fourier expansions in the azimuthal direction. Lagrange elements of degree 1 to approximate $\mathbf{H}^c$ in the conducting region and Lagrange elements of degree 2 to approximate ϕ in the non-conducting-region lead to $\mathcal{O}(h^{3/2})$ error in the L^2-norm of the magnetic field.

Our algorithm is limited to simply connected non-conducting domains for the time being or tori with zero net current. Actually, using a scalar potential ϕ to represent the external magnetic field is possible as soon as the circulation of the magnetic field vanishes around every closed path in the vacuum. This is indeed the case for time-dependent dynamo computations starting with a potential initial magnetic field. In this case the induced fields and currents are on mode $m \neq 0$, and the net current on mode $m = 0$ stays equal to zero. Thus, although the present algorithm is not yet capable of simulating tokamak MHD problems (which have net

toroidal currents), it can be used for simulating conducting flows in a torus like we did for the Perm device [11]. Note also that the algorithm can deal with spatial distributions for σ and μ and that opens new perspectives for studying more realistic configurations.

We have studied Ohmic decay in axisymmetric compact conducting regions such as a sphere and ellipsoids. The algorithm may also be directly used for a much larger variety of applications of practical interest, after proper selection of the boundary conditions and adapting the mesh to the topology of the problem. For example, computations of induction in a rotating infinite or finite cylinder are reported in [20]. This code is also able to describe the kinematic dynamo acting in axisymmetric finite containers as presented in Section 5.2, including conductivity jumps.

After coupling the present code with its FEM hydrodynamical counterpart, which is now available, we will be ready to examine nonlinear MHD phenomena occurring in realistic configurations.

Acknowledgments

We are deeply grateful to the organizers of the summer MHD program 2005 at Université Libre de Bruxelles, D. Carati, S. Kassinos and B. Knaepen where part of the runs was performed. We acknowledge fruitful discussions with W. Dobler, P. Frick and R. Stepanov. R.L. is thankful to Texas A&M University for supporting him in 2005.

References

[1] A. Alonso, A mathematical justification of the low-frequency heterogeneous time-harmonic Maxwell equations, Math. Models Methods Appl. Sci. 9 (3) (1999) 475–489.
[2] D.N. Arnold, An interior penalty finite element method with discontinuous elements, SIAM J. Numer. Anal 19 (1982) 742–760.
[3] G.A. Baker, Finite element methods for elliptic equations using nonconforming elements, Math. Comp. 31 (137) (1977) 45–59.
[4] A. Bossavit, Magnetostatic problems in multiply connected regions: some properties of the curl operators, Proc. Inst. Elec. Eng. 135 (1988) 179–187.
[5] A. Bossavit, The computation of eddy-currents, in dimension 3, by using mixed finite elements and boundary elements in association, Math. Comput. Modelling 15 (3–5) (1991) 33–42.
[6] A. Bossavit, Computational Electromagnetism, Variational Formulations, Complementary, Edge ElementsElectromagnetism, vol. 2, Academic Press, New York, 1998.
[7] R. Bramley, X. Wang, Splib: a library of iterative methods for sparse linear system. Technical Report, Indiana University – Bloomington, Bloomington, IN 47405, 1995.
[8] H. Brezis, Analyse Fonctionnelle, Masson, Paris, 1991.
[9] B. Cockburn, C.W. Shu, The local discontinuous Galerkin method for time-dependent convection–diffusion systems, SIAM J. Numer. Anal. 35 (1998) 2440–2463.
[10] M. Costabel, A coercive bilinear form for Maxwell's equations, J. Math. Anal. Appl. 157 (2) (1991) 527–541.
[11] W. Dobler, P. Frick, R. Stepanov, Screw dynamo in a time-dependent pipe flow, Phys. Rev. E 67 (2003) 056309.
[12] P. Dular, C. Geuzaine, Modeling of thin insulating layers with 3D magnetodynamic formulations, IEEE Trans. Magn. 39 (2003) 1139–1142.
[13] P. Frick, V. Noskov, S. Denisov, S. Khripchenko, D. Sokoloff, R. Stepanov, A. Sukhanovsky, Non-stationary screw flow in a toroidal channel: way to a laboratory dynamo experiment, Magnetohydrodynamics 38 (1–2) (2002) 143–162.
[14] J.-L. Guermond, J. Léorat, C. Nore, A new finite element method for magneto-dynamical problems: two-dimensional results, Eur. J. Mech./Fluids 22 (2003) 555–579.
[15] J.-L. Guermond, P.D. Minev, Mixed finite element approximation of an MHD problem involving conducting and insulating regions: the 2D case, Modél. Math. Anal. Numer. (M2AN) 36 (3) (2002) 517–536.
[16] J.-L. Guermond, P.D. Minev, Mixed finite element approximation of an MHD problem involving conducting and insulating regions: the 3D case, Numer. Methods Partial Differential Eq. 19 (6) (2003) 709–731.
[17] A.B. Iskakov, S. Descombes, E. Dormy, An integro-differential formulation for magnetic induction in bounded domains: boundary element-finite volume method, J. Comput. Phys. 197 (2) (2004) 540–554.
[18] J. Zou, K.H. Chan, K. Zhang, G. Schubert, A non-linear, 3-D spherical α^2 dynamo using a finite element method, Phys. Earth Planetary Interiors 128 (2001) 35–50.
[19] R. Laguerre, C. Nore J. Léorat, J.-L. Guermond, Effects of conductivity jumps in the envelope of a kinematic dynamo flow, C. R. Mécanique, in press.
[20] R. Laguerre, C. Nore, J. Léorat, J.-L. Guermond, Induction effects in isolated axisymmetric conductors using a new finite element method, in: D. Carati, B. Knaepen (Eds.), Proceedings of the Bruxelles ULB MHD Workshop, Bruxelles, July 2005.
[21] J.-L. Lions, E. MagenesProblèmes aux limites non homogènes et applications, vol. 1, Dunod, Paris, 1968.

[22] H.K. Moffatt, Magnetic Field Generation in Electrically Conducting Fluids. Cambridge Monographs on Mechanics and Applied Mathematics, Cambridge University Press, Cambridge, 1978.
[23] Ilaria Perugia, Dominik Schötzau, The hp-local discontinuous Galerkin method for low-frequency time-harmonic Maxwell equations, Math. Comp. 72 (243) (2003) 1179–1214 (electronic).
[24] S. Rebay, Efficient unstructured mesh generation by means of Delaunay triangulation and Bowyer–Watson algorithm, J. Comput. Phys. 106 (1993) 125–138.